

On Palaeozoic–Mesozoic brittle normal faults along the SW Barents Sea margin: fault processes and implications for basement permeability and margin evolution

Kjetil Indrevær^{1,2,*}, Holger Stunitz¹ & Steffen G. Bergh¹

1) Department of Geology, University of Tromsø, N-9037 Tromsø, Norway

2) DONG E&P Norge AS, Roald Amundsens Plass 1, N-9257 Tromsø, Norway

* Corresponding author (e-mail: kjetil@indrevar.no)

Abstract: Palaeozoic–Mesozoic brittle normal faults onshore along the SW Barents Sea passive margin off northern Norway give valuable insight into fault and fluid flow processes from the lower brittle crust. Microstructural evidence suggests that Late Permian–Early Triassic faulting took place during multiple phases, with initial fault movement at minimum P – T conditions of $c.$ 300 °C and $c.$ 240 MPa ($c.$ 10 km depth), followed by later fault movement at minimum P – T conditions of $c.$ 275 °C and $c.$ 220 MPa ($c.$ 8.5 km depth). The study shows that pore pressures locally reached lithostatic levels (240 MPa) during faulting and that faulting came to a halt during early (deep) stages of rifting along the margin. Fault permeability has been controlled by healing and precipitation processes through time, which have sealed off the core zone and eventually the damage zones after faulting. A minimum average exhumation rate of $c.$ 40 m Ma⁻¹ since the Late Permian is estimated. It implies that the debated Late Cenozoic uplift of the margin may be explained by increased erosion rates in the coastal regions owing to climate deterioration, which caused subsequent isostatic recalibration and uplift of the marginal crust. The studied faults may be used as analogues of basement-involved fault complexes offshore, revealing details about the offshore nature of faulting, including past and present basement and fault zone permeability.

Introduction

It is well known that the strength of the crust depends not only on the frictional strength of dry rocks, but also on pore pressure at depth (e.g. Hubbert & Rubey 1959). The consequence is that the brittle strength of the crust can be of the order of several hundred MPa under hydrostatic pore pressure conditions (depending on depth) or negligible as pore pressures approach lithostatic values (Sibson 1973; Byerlee 1978; Brace & Kohlstedt 1980; Jaeger *et al.* 2009). The importance of this effect on crustal strength was first fully appreciated when attempts to model earthquakes had to involve fluids to replicate the strength of the brittle crust (e.g. Sibson *et al.* 1975; Sibson 1977, 1989; Byerlee 1990, 1993; Zoback 1991; Rice 1992; Blanpied *et al.* 1992; Bruhn *et al.* 1994). These models implied that pore pressures within fault zones were commonly elevated, also at deeper levels of the seismogenic zone.

Several studies have since discovered that faults act as important pathways for fluids in the upper crust as they represent high-permeability zones owing to fracturing and cataclasis (e.g.

Sibson 1973, 1977; Hickman *et al.* 1995; Seront *et al.* 1998; Gudmundsson *et al.* 2001; Zoback & Townend 2001; Crampin *et al.* 2002; Ganerød *et al.* 2008). Experimental data have shown that fluid-involved processes, which control fault strength and permeability, include fault healing through pressure solution and hydrothermal precipitation of minerals (Karner *et al.* 1997; Olsen *et al.* 1998; Bos & Spiers 2000; Kanagawa *et al.* 2000; Nakatani & Scholz 2004). However, observations and analysis of fault rock, fluid interactions and fluid behaviour (including fluid pore pressure) from natural examples are relatively scarce in the literature (e.g. Bruhn *et al.* 1994; Eichhubl & Boles 2000; Caine *et al.* 2010; Faulkner *et al.* 2010). In particular, this appears to be the case for preserved examples from the deeper parts of the seismogenic zone (5–12 km), which are crucial to understand fault and fault–fluid behaviour at depth (see Faulkner *et al.* 2010).

In the present study, we present observations from naturally occurring fault rocks, which show evidence for elevated pore pressure and fluid flow during faulting in the deeper parts of the seismogenic zone. The fault zones crop out as a network of Late Permian–Early Triassic brittle normal faults in Troms, northern Norway (Fig. 1; Andresen & Forslund 1987; Forslund 1988; Opheim & Andresen 1989; Olesen *et al.* 1997; Davids *et al.* 2013; Indrevær *et al.* 2013) and constitute major fault complexes that run partly onshore, partly offshore along the SW Barents Sea passive margin (Indrevær *et al.* 2013). The fault zones display mostly Permian–Early Triassic ages of faulting (Davids *et al.* 2013) and varying amounts of displacement (>3 km to <100 m) (Forslund 1988; Opheim & Andresen 1989; Olesen *et al.* 1997; Indrevær *et al.* 2013). We describe and characterize features indicating fault–fluid interactions and high pore pressures in fault rocks from selected onshore fault zone outcrops in the region (Fig. 2), and we aim to estimate P – T conditions and fluid pressures during faulting from mineral assemblages and microstructures. This approach may yield insight into important processes operating during faulting in the intermediate to deeper levels of the brittle crust (<15 km). The implications of syn- and post-deformation fault rock permeability will be discussed in the context of the potential for hydrocarbon migration and entrapment within basement rocks in the region. Lastly, the results will be set into context with the current understanding of evolution of the SW Barents Sea passive margin (see Gabrielsen *et al.* 1990; Faleide *et al.* 2008; Smelror *et al.* 2009).

Geological Setting

The studied fault rock outcrops are located within the West Troms Basement Complex, a basement horst situated on the SW Barents Sea margin, northern Norway (Fig. 1). The horst is

bounded by the Lofoten igneous and high-grade metamorphic province to the SW (Corfu 2004) and by largely Permian–Early Triassic high-angle normal faults, which down-drop Caledonian nappes, to the east (Andresen & Forslund 1987; Zwaan 1995; Davids *et al.* 2013; Indrevær *et al.* 2013). The West Troms Basement Complex is made up of various Meso- and Neoproterozoic tonalitic, trondhjemitic and granitic gneisses and meta-supracrustal belts, intruded by felsic and mafic igneous rocks (Corfu *et al.* 2003; Bergh *et al.* 2010).

The Permian–Early Triassic rift-related activity in the region is manifested within the horst by widespread NNE–SSW- and ENE–WSW-trending brittle normal faults and fractures arranged in a zig-zag pattern along the southeastern and northwestern limits of the West Troms Basement Complex. A subsidiary NW–SE-trending fracture system is also present (Fig. 1; see Indrevær *et al.* 2013). The onshore fault zones can be divided into the Vestfjorden–Vanna Fault Complex, which marks the southeastern boundary of the West Troms Basement Complex, down-dropping Caledonian nappes to the east by some 1–3km (Forslund 1988; Opheim & Andresen 1989; Olesen *et al.* 1997), and a less prevalent, SE-dipping, segmented fault array that runs along the outer rim of the islands of the West Troms Basement Complex (Antonsdóttir 2006; Thorstensen 2011; Indrevær *et al.* 2013) with displacement of the order of hundreds of metres or less (Indrevær *et al.* 2013; Fig. 2).

The northwestern limit of the West Troms Basement Complex is identified as the Troms–Finnmark Fault Complex (Indrevær *et al.* 2013), which runs offshore, parallel to the West Troms Basement Complex, where basement is down-faulted more than 5km in the Harstad Basin, to *c.* 10km depth (Fig. 1; Indrevær *et al.* 2013). Preserved Caledonian nappes thrust on top of Precambrian basement, as observed in the mainland of northern Norway, are indicated to be present within large regions of the SW Barents Sea (Gernigon & Brønner 2012) and may be present offshore from the West Troms Basement Complex, overlying down-faulted Precambrian basement.

The Troms–Finnmark and Vestfjorden–Vanna fault complexes (Figs 1 and 2) can be traced for hundreds of kilometres along strike of the north Norwegian margin, linking up major structural elements in the south, such as the Lofoten and Nordland ridges, with offshore fault complexes in the north, such as the Ringvassøy–Loppa, Nysleppen and Måsøy fault complexes (Doré *et al.* 1997, 1999; Olesen *et al.* 1997; Indrevær *et al.* 2013). Because the Vestfjorden–Vanna Fault Complex, which runs partly onshore, links up with offshore fault complexes, the fault zones in western Troms act as a unique natural laboratory for studying

offshore-correlative basement-seated fault zones and their characteristics.

Timing of faulting

Ages of onshore rocks and fault rocks derived using the $^{40}\text{Ar}/^{39}\text{Ar}$ and/or apatite fission-track methods are interpreted to indicate that faulting in western Troms largely occurred in the Permian to Early Triassic with insignificant fault displacement or reactivation later in the Mesozoic and Cenozoic (Hendriks *et al.* 2010; Davids *et al.* 2013). Instead, Mesozoic fault activity took place offshore, along the Troms–Finnmark Fault Complex (Gabrielsen *et al.* 1990), further north in Finnmark (Roberts & Lippard 2005; Torgersen *et al.* 2013) and to the south in Vesterålen and Andøya (Dalland 1981; Fürsich & Thomsen 2005; Eig 2008; Hansen 2009; Hendriks *et al.* 2010; Osmundsen *et al.* 2010; Davids *et al.* 2013). The onshore faults in Troms are therefore believed to have been abandoned after the Late Permian–Early Triassic rifting phase and thus reflect conditions of early stages of rifting (Davids *et al.* 2013; Indrevær *et al.* 2013). However, palaeomagnetic evidence for Permian as well as Cenozoic to recent phases of faulting has been obtained for fault segments within the Vestfjorden–Vanna Fault Complex in Troms (Olesen *et al.* 1997), suggesting that the major offshore fault activity triggered minor reactivation on some onshore faults.

Methods

Several fault segments with good outcrops of fault rocks in the West Troms Basement Complex have been investigated through structural mapping, including extensive sampling of rocks from both the core zones and damage zones. Fault rock studies using polarizing light microscopy and SEM analysis, including backscatter detection (BSD) and energy-dispersive spectrometry (EDS), have been conducted to identify mineral assemblages, which have been used in estimation of P – T conditions during faulting, and to identify and describe fault rocks to provide insight into fault and fluid flow characteristics.

Results

Described fault segments with distinct fault rocks include the Rekvika, Bremneset, Tussøya and Kvaløysletta–Straumbukta fault zones (Fig. 2; Forslund 1988; Opheim & Andresen 1989; Olesen *et al.* 1997; Antonsdóttir 2006; Thorstensen 2011; Indrevær *et al.* 2013). These and other fault rocks of the West Troms Basement Complex have been mapped and discussed in a regional context by Indrevær *et al.* (2013). The Rekvika, Bremneset and Tussøya faults have estimated amounts of displacement of the order of hundreds of metres or less (Indrevær

et al. 2013). The Kvaløysletta–Straumsbukta fault zone is a fault segment of the Vestfjorden–Vanna Fault Complex with an estimated amount of displacement of 1–3 km (Forslund 1988). In the following, we aim to describe the meso- and microscopic petrological characteristics of the fault rocks from these fault zones as a basis for discussing P – T conditions, fault evolution, fluid flow characteristics, and fluid pressures during faulting.

Rekvika fault zone

Mesoscale observations. The sinistral-normal Rekvika fault zone (Fig. 2, map A; Antonsdóttir 2006; Indrevær *et al.* 2013) dips SE and cuts through parts of a granitic intrusion. The damage zone ranges in width from 30 to 50m into the footwall, consisting mainly of protocataclastic red stained granite. It is abundantly cut by irregular quartz veins and enriched in epidote (Fig. 3a and b). The process zone occurs as a *c.* 2 m wide, light green, ultracataclasite composed of dominantly quartz and minor hematite (Fig. 3c). The ultracataclasite is cut by later irregular quartz veins (Fig. 3c). Both the hanging wall and the footwall are characterized by a >400m wide zone along strike of conspicuous red staining of the granite (Fig. 3d).

Microscale observations. In thin section, at least three generations of cataclasites are observed within the light green core zone (Fig. 3e and f). The first generation cataclasite is preserved as sub-angular 0.2– 1mm clasts of very fine-grained quartz ultracataclasite (internal grain size of 5 μ m to <1 μ m) containing *c.* 99% quartz and 1% hematite. The first generation cataclastic aggregates are embedded within rounded to sub-rounded clasts of a second generation of quartz ultracataclasite (Fig. 3e and f), which is composed of *c.* 80% quartz and *c.* 20% hematite. The sub-rounded clasts of the second generation are, again, embedded within a third generation, composed of 99% quartz and less than 1% hematite with a grain size in the range from 50 μ m to <1 μ m. The fine-grained domains show microstructural characteristics of healing and grain growth, evident from the development of cusped grain boundaries (Fig. 3g), indicating that the initial clast grain size was less than what is observed in thin section.

Later extensional fractures with infill of quartz cut both generations of cataclasites (Fig. 3e and f). These fractures are cut first by fractures containing both hematite and quartz, and subsequently by fractures showing only hematite. A lens of mafic gneiss that shows an amphibolite-facies mineral assemblage away from the fault zone (Fig. 2, map A) is statically retrograded to chlorite (60%), quartz (30%), epidote (5%), albite (5%), and accessory titanite and muscovite within the damage zone of the fault zone (Fig. 3h).

Tussøya fault zone

Mesoscale observations. This sinistral-normal fault zone dips moderately ESE and separates granite in the footwall from banded mafic and felsic gneisses in the hanging wall (Fig. 2, map B and Fig. 4a; Indrevær *et al.* 2013). The fault crops out as a 1–3 m thick proto- to ultracataclastic zone (Fig. 4b). The granite in the footwall is stained red, similar to the Rekvika fault zone, within a 200 m wide zone and is commonly cut by dark bands of ultracataclasite (Fig. 4c). Altered granite also occurs in the hanging wall in the southern parts of the outcrop area. Subsidiary, ENE–WSW-trending, dextral normal faults interact with the overall main NNE–SSW fault trend and are displaced by the main fault. In general, the footwall is more deformed than the hanging wall.

The dark bands of ultracataclasite are injected into fractures in the sidewall of the faults (Fig. 4c and d). These injections show a lack of internal foliation, indicating no significant amount of displacement along the fracture, which would be needed to produce the observed cataclasite *in situ*, and a lack of any significant damage to the side-walls of the fracture. Also, the fractures that are filled with cataclasites are commonly at high angles to the main fault zone. However, the fractures do have some displacement along them, as the side-walls of the fracture do not match up properly (Fig. 4d).

Microscale observations. Within the core zone, at least three generations of cataclasites are observed in thin sections (Fig. 4e and f). The oldest generation consists of angular to sub-rounded clasts, 5 mm to <1 µm in size, made up of quartz (90%) and feldspar (10%) within a matrix composed of quartz (80%), epidote (20%) and accessory hematite (Fig. 4e and f). The second generation is characterized by sub-angular to rounded clasts of quartz (90%) and feldspar (20%) within a matrix of epidote (40%), hematite (30%), quartz (20%) and chlorite (10%) (Fig. 4e and f). The third generation of cataclasite is observed in association with microfaults, which cut the two previous generations (Fig. 4e and f) and consist of quartz (60%), albite (30%), pumpellyite (10%) and hematite (1%).

Microstructural study of the inferred injected ultracataclasites confirms the lack of any high-strain zone within the cataclasite, supporting its injected nature inferred from outcrop observations. The ultracataclasites have formed elsewhere (probably along larger fault segments) and been transported into fractures (Fig. 4g and h), resulting in the dark bands of ultracataclasites observed in outcrops (Fig. 4d).

Within the damage zone, biotite is locally fractured and dilated by the precipitation of quartz

(Fig. 5a). Larger clasts of quartz show undulatory extinction (Fig. 5b) and both quartz and feldspar show healed fractures, with nucleation of new grains along the healed fractures (Fig. 5b and c). Comparing unaltered and altered granite under a polarizing microscope reveals that the red staining is limited to grains of plagioclase (Fig. 5d–g). Micro-grains of iron oxides (<1 μm in size) in larger plagioclase grains produce the red staining (Fig. 5f and g).

Bremneset fault zone

Mesoscale observations. This normal fault (Fig. 2, map C) dips ESE and occurs as a 0–3 m thick cataclastic zone that can be traced along the shore for *c.* 200m, cutting migmatitic, banded gneisses (Fig. 6a and b). The gneiss foliation is in general at a moderate angle to the fault zone. Fault and fracture surfaces commonly show epidote precipitation, and they are locally cut by younger faults or fractures with hematite staining. The core zone is composed of epidote-rich cataclasite with minor quartz and chlorite (Fig. 6b).

Microscale observations. A fractured amphibolite gneiss from the damage zone of the Bremneset fault zone consists of albite (40%), quartz (30%), chlorite (5%), epidote (5%), apatite (1%) and accessory titanite and calcite (Fig. 6c and d). Clasts of fractured epidote (Fig. 6e) show typical grain growth features including the formation of idiomorphic grain boundaries. Later faulting has fractured the annealed epidote grains. EDS analysis shows that pumpellyite occurs along these fractures (Fig. 6f and g). Chlorite grains are observed being fractured and dilated by titanite infill (Fig. 6h).

Plagioclase grains are commonly stained red, but the staining is not present along healed fractures when they cut plagioclase grains (see Fig. 5f and g). Preserved larger quartz and feldspar grains show traces of healed fractures similar to those in the Tussøya fault zone (Fig. 5c and d). The larger quartz grains show undulatory extinction. Late-stage microfaults cut the cataclasite without forming new cataclasite along the faults (Fig. 7a and b). Within healed fractures, fluid inclusions are observed, indicating the presence of fluids during fracturing.

Away from the Bremneset fault zone, viscously deformed amphibolites are preserved outside the fault zones. Foliation-parallel plastically boudinaged quartz veins are commonly found within the gneisses. As they are boudinaged, they clearly predate the brittle deformation (Fig. 7c). Approaching the fault zone, the amphibolite-facies ductile microstructure is progressively retrograded to a greenschist-facies mineral assemblage through static recrystallization, except in zones around the boudinaged quartz veins (Fig. 7d and e). As static retrogression is indicative of the percolation of fluids through the rock, the preserved amphibolite-facies

metamorphic mineral assemblage along the outer rim of the quartz veins indicates that the quartz veins have prevented fluid flow across these zones.

Kvaløysletta–Straumbukta fault zone

Mesoscale observations. This is an oblique-dextral normal fault zone (Fig. 2, map D; Forslund 1988; Olesen *et al.* 1997; Indrevær *et al.* 2013), which dips SE and runs along the eastern rim of Kvaløya, juxtaposing Precambrian gneisses in the footwall and Caledonian nappes in the hanging wall. Near Straumbukta, parts of the footwall damage zone crop out within foliated tonalitic and amphibolitic gneisses (Fig. 8a and b). Fault surfaces commonly trend north–south and locally NE–SW, and are parallel to a moderately east-dipping foliation in the gneisses. The footwall outcrop is increasingly deformed towards the east. The tonalitic gneisses are commonly stained red, as observed along the other studied fault zones. In outcrops, related fault and fracture surfaces are coated with chlorite and quartz, and systematically are cut by fractures coated with hematite.

Microscale observations. At least two generations of cataclasites are observed in mafic rocks of the damage zone in Straumbukta. The first generation consists of very fine-grained (<1 µm) epidote (40%), chlorite (40%) and quartz (20%) aggregates, which appear as clasts within a second generation of cataclasite composed of quartz (50%), chlorite (30%) and epidote (20%) in the matrix (Fig. 8c and d). Chlorite within the second generation of cataclasite commonly shows radial growth (Fig. 8e and f). Both generations of the fault rocks are cut by quartz and chlorite veins, in successive order.

Plagioclase grains from the tonalitic gneisses of the damage zone are commonly stained red, similar to the other studied fault zones. Notably, the plagioclase within the amphibolite gneisses is retrograded to sericitic albite with overgrowth of white mica and epidote, which is also present within amphibolitic gneisses from Bremneset (Fig. 7d).

In summary, a common feature to all of the studied fault zones and related fractures is the red staining of plagioclase within the fault damage zone and hydrothermal precipitation of epidote, quartz, chlorite, calcite and/or hematite along fracture surfaces and in the matrix of cataclasites. Cross-cutting relationships demonstrate that epidote, quartz and chlorite veins formed first and were later cut by veins composed dominantly of hematite. At least two generations of cataclasites were formed during faulting, accompanied by mineral recrystallization and/or growth. Both the cataclasites and the statically recrystallized mafic gneisses show the mineral assemblage epidote + quartz + chlorite + albite + titanite ± apatite

± calcite ± muscovite. Subsequent fracturing and cataclasis introduced pumpellyite to the mineral assemblage.

Discussion

P–T conditions during faulting

The mineral assemblage epidote + quartz + chlorite + albite + titanite ± apatite ± calcite ± muscovite is identified in the first generations of cataclasites in mafic gneisses of the Bremneset and Tussøya fault zones. This mineral assemblage indicates that greenschist-facies metamorphic conditions were present during faulting. The same mineral assemblage is observed in statically recrystallized mafic gneisses from the damage zones of the Rekvik and Bremneset fault zones. The formation of pumpellyite in later-stage fractures in cataclastic mafic gneisses at Bremneset and in granitoid fault rocks at Tussøya further suggests decreasing *P–T* conditions of faulting through time, as pumpellyite is stable at sub-greenschist-facies conditions.

The presence of greenschist-facies mineral assemblage (epidote + quartz + albite + chlorite ± white mica) is indicative of a minimum temperature during the formation of the early generations of cataclasites at *c.* 300 °C (Fig. 9; Bucher & Grapes 2011). Fractured grains of epidote show grain growth and the development of idiomorphic grain boundaries (Fig. 6e). As grains of epidote are fractured, this implies that epidote and thus, greenschist-facies metamorphic conditions, were reached prior to fracturing. The post-fracturing grain growth and the development of idiomorphic grain boundaries of the fractured epidote indicate that greenschist-facies metamorphic conditions persisted after the early event(s) of brittle faulting. Later fault movement fractured the idiomorphic grains, and fine-grained pumpellyite formed along these fractures. Pumpellyite forms at temperatures ranging from *c.* 250 to 300°C (Fig. 9; Bucher & Grapes 2011). Thus, the presence of pumpellyite suggests that the temperature decreased below *c.* 300 °C during later stages of faulting.

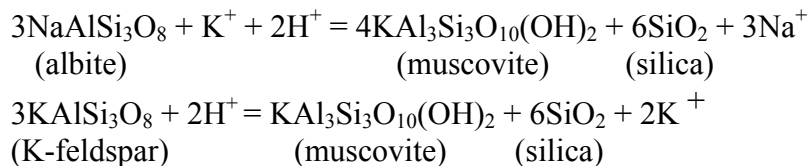
The observed microstructures and greenschist-facies mineral assemblages do not allow for a precise estimate of confining pressure during deformation owing to the relatively wide pressure range of stability for greenschist-facies assemblages. The occurrence of pumpellyite, however, yields a minimum pressure for the later-stage faulting of *c.* 220MPa corresponding to a minimum depth of *c.* 8.5 km, assuming an average meta-MORB (mid-ocean ridge basalt) composition of the amphibolites and an upper lithospheric density of 2600 kg m⁻³ (Fig. 9).

From these estimates, it is possible to infer the highest possible geothermal gradient during the time of faulting as *c.* 30 °C km⁻¹.

A minimum estimate for pressures during the earlier greenschist-facies fault activity may be obtained by extrapolating this geothermal gradient up to *c.* 300°C (the minimum temperature estimate for the greenschist faulting conditions). This yields a minimum pressure of the early stage faulting at *c.* 245MPa, corresponding to *c.* 10 km depth (Fig. 9).

Fault rocks and fluid interactions

The Rekvika and Tussøya fault zones run partly within granitic rocks. Fault zones within feldspar-rich host rocks commonly develop phyllonites within core zones of faults, as a result of the breakdown of feldspars to phyllosilicates (Wintsch *et al.* 1995; Janecke & Evans 1988; Wibberley 1999; Rutter *et al.* 2001; Holdsworth 2004; Jefferies *et al.* 2006). In Rekvika and Tussøya, however, the formation of phyllonites within the core zones is not observed. Rather, within the core zone of the Rekvika fault zone, a *c.* 2 m wide zone of quartzitic ultracataclasite occurs. Wibberley (1999) described preserved clasts of ‘cemented quartz–albite-ultracataclasite’ within phyllonites and attributed them to early stages of faulting, where the chemical breakdown of orthoclase feldspars to muscovite leads to the release of quartz. The chemical reactions are (Wibberley 1999)



These reactions are favoured in meteoric water-dominated granitic fault systems (Wintsch *et al.* 1995).

The occurrence of the quartzitic ultracataclasite at Rekvika may thus be preserved early stages of faulting, which, in contrast to the Wibberley (1999) study, are preserved where these fault rocks form relict clasts within phyllonites. If so, at least three generations of such cataclasites can be observed in Rekvika and suggest that the fault zone was abandoned after early stages of rifting so that subsequent fault activity and progressive formation of phyllosilicates (inducing fault weakening) did not occur.

Within the Rekvika and Tussøya fault zones, no extensive formation of muscovite is observed, as would be predicted if the abundance of quartz within the core zone of the

(Putnis *et al.* 2007) or iron-rich plagioclase, where albitization of plagioclase leads to exsolution of iron from the plagioclase crystal at lower temperatures, and its reaction and oxidization in contact with fluids to form distributed hematite (Tegner 1997). Our microstructural studies also suggest that some of the iron may originate from biotite, which has retrograded to chlorite.

Healed fractures cutting plagioclase pseudomorphs are observed to have narrow zones without red staining along them. This indicates that, during later stages of fluid flow, fluids permeated through the fractures as they opened and removed hematite along the now healed fractures (Fig. 5f and g). This may explain the enrichment of hematite within some of the cataclasites and the wide occurrence of later stage precipitation of hematite on fault and fracture surfaces. The ubiquitous epidote in addition to the abundant hematite suggests that conditions were oxidizing during faulting.

Pore pressure and stress conditions

Pore pressure is a critical controlling factor of crustal strength. High pore pressure will effectively decrease the confining pressure and, depending on the differential stress, fracturing will occur as pore pressure approaches lithostatic values (e.g. Hubbert & Rubey 1959; Haimson & Fairhurst 1967). In the following, we will discuss observations that are consistent with fluids having dilated or created open space within the fault rocks, which is indicative of lithostatic pore pressures during faulting. For simplicity, we define lithostatic pressure as equal to σ_3 .

The microstructural observations include the following.

(1) Mineral precipitation on fault or fracture surfaces. For fluids to hold fractures open (at least by very small amounts) to allow precipitation of minerals in the dilatant sites, the fluid pressure must exceed the normal stress acting on a fracture plane and as a minimum, be equal to σ_3 (Delaney *et al.* 1986).

(2) Fracturing and dilatation. Microstructural evidence for fracturing and dilatation of the fault rocks is observed and interpreted in the form of fractured biotite with injection of fluids and precipitation of quartz (Fig. 5g), and fractured chlorite with injection of fluids and precipitation of titanite (Fig. 6h). For fluid injection and crack dilatation, the pore pressure needs to equal or exceed σ_3 .

(3) Radial growth of chlorite within cataclasites. Undeformed (and thus post-faulting) radial aggregates of chlorite are observed in thin section (Fig. 8f). The radial shape suggests that it has grown into an open pore space. For pore space to exist at depth, the pore pressure must, as a minimum, have been equal to σ_3 .

(4) Injection of ultracataclasite into the host rock. As pore pressures were sufficient for opening veins for cataclasites to be injected during deformation (Figs 4c, d, g and h), the pore pressure must, as a minimum, have reached σ_3 .

Owing to the above-mentioned indications for pore pressures reaching σ_3 , a minimum estimate of the pore pressure during faulting is thus *c.* 240MPa, corresponding to the pressure of deformation obtained from estimations based on mineral assemblages from earlier sections. It follows that the differential stress must have been relatively low for the fluid pressure to have reached lithostatic values without causing hydraulic fracturing during earlier phases of pore pressure build-up. Assuming a typical Mohr–Coloumb failure criterion (see Goodman 1989), the differential stress needed to fracture a rock that is subjected to lithostatic pore pressure is of the order of tens of MPa at the most (Fig. 10). The inferred lithostatic pore pressure thus implies that the middle crust was relatively weak during faulting.

The high pore pressure within the fault zones may be explained by episodic flow of high-pressure fluids, also known as seismic pumping (e.g. Sibson *et al.* 1975; Byerlee 1993). The cyclic nature of seismic pumping fits with the inference of episodic rupture in the studied fault zones as suggested by the range of mineral precipitates and several generations of cataclasites.

Fluid flow velocity

The presence of injected ultracataclasites into veins of the fault rocks (Fig. 4g and h) provides an opportunity to roughly estimate the co-seismic fluid velocity during faulting and injection. For cataclasites to be injected, they need to be fluidized.

Stokes' Law, describing the settling of a sphere, provides a good approximation to the fluidization velocity of a granular material (Rodrigues *et al.* 2009). Fluidizing occurs as the fluid velocity (V) surpasses the settling velocity (U) of a granular material. The minimum fluid flow needed to fluidize and inject the observed ultracataclasite is

$$V \geq U = \frac{2(\rho_s - \rho_f)gR^2}{9\mu}$$

where ρ_s and ρ_f are the density of a sphere (clast) and fluid, respectively, g is the gravitational constant, R is the radius of a sphere (clast), here set to 100 μ m as observed in thin section (Fig. 5g and h), and μ is the dynamic viscosity, set to 10⁻⁴ kg m⁻¹ s⁻¹ for water (for simplicity) at 300 °C (Schmidt & Mayinger 1963). We obtain a value on the order of 10⁻¹ m s⁻¹ using the parameters derived from this study.

Eichhubl & Boles (2000) calculated palaeo-fluid flow rates during co-seismic fluid expulsion events of a minimum of 0.01 m s⁻¹. The value obtained in the present study suggests that co-seismic rates of fluid flow may exceed those estimated by Eichhubl & Boles (2000) by one order of magnitude.

Fault zone permeability

The above discussion supports that the studied fault zones have acted as fluid conduits during faulting. In addition to their conduit properties such as grain growth and mineral precipitation, other microstructural observations have been made, which shed light on pre- and syn-faulting basement rock permeability.

First, the observed static recrystallization of pre-existing, Archaean–Proterozoic amphibolite-facies ductile fabrics, which are retrograded to greenschist-facies minerals, indicates that fluid infiltration has taken place in the adjacent gneisses. Consequently, permeability within the basement rocks must have been sufficiently large to allow for adequate fluid flow through the rock. Furthermore, basement permeability prior to the brittle deformation has been highly anisotropic, as illustrated by the impregnating properties of pre-existing, boudinaged, foliation-parallel quartz veins (Fig. 7c–e), which have protected its immediate surroundings from static retrogradation, hence limiting permeability across the vein. Thus, pre-existing, extensive, foliation-parallel quartz veining will allow for fluid flow parallel to foliation, but impede across-foliation fluid flow.

Second, the large amount of precipitation of hydrothermal minerals on fault and fracture surfaces in the damage and process zones implies that the fault zones have acted as fluid transport paths. The red staining of feldspar-rich host rocks may also influence fault zone permeability. Drake *et al.* (2008) have shown that the red staining process of plagioclase pseudomorphs increases the porosity compared with unaltered samples. This implies that, as

fluid infiltration and red staining occurs in a plagioclase-rich rock, the permeability within these hydrothermally altered zones will increase with time, as more plagioclase grains are pseudomorphed, giving a positive feedback mechanism for the red staining process.

A model is proposed, using the terminology of fluid flow characteristics of Caine *et al.* (1996), describing faults as fluid conduits, fluid barriers, or fluid conduit–barriers (Fig. 11). The model summarizes the observed feedback mechanisms that may influence fault zone permeability by illustrating the dynamic evolution of three end-member fault zones: (1) a fault zone within granitic host rocks (the Rekvika fault zone); (2) a fault zone within foliated gneisses (the Bremneset fault zone); (3) a fault zone separating granitic rocks in the footwall from banded gneisses in the hanging wall (the Tussøya fault zone).

Prior to faulting, the permeability with granites is assumed to be isotropic. Within sub-horizontal banded gneisses, the horizontal permeability is assumed similar to the permeability within granites, whereas the vertical permeability is strongly impeded owing to pre-existing, impermeable foliation-parallel layers, such as quartz veins. The observed microstructures suggest that, as faulting initiates, fracturing and cataclasis in the core zone and immediate damage zone leads to an increase in permeability and hence an increase in vertical fluid flow within the central parts of the fault (Fig. 11a). As silica walls form owing to pressure release, the permeability within the core zone decreases rapidly and this zone probably becomes completely sealed. The trapped fluids are forced into the surrounding damage zone (Fig. 11b). Here, fluid flow is more restricted, but increases through time within feldspar-rich host rocks, as the red staining process increases permeability. Thus, the damage zone will become the preferred fluid pathway for along-fault fluid flow during periods after faulting (Fig. 11b). In the banded gneisses, however, any vertical (along-fault) fluid flow will be restricted by impermeable foliation-parallel layers and thus encourage foliation-parallel fluid flow away from the fault zone. During longer periods of fault quiescence, a number of subsidiary factors, such as later grain growth, the sealing of fractures and secondary mineral growth–precipitation on fracture surfaces and within pore space, will completely seal the fault zones, impeding both vertical and horizontal fluid flow, independent of host-rock lithology (Fig. 11c). Keulen *et al.* (2008) have shown, based on microstructural criteria, that such healing may occur within a few months at 300°C, through the processes of dissolution and grain growth. Any later reactivation of the fault zone, however, may restart the above-described cycle (Fig. 11a–c). The model implies that a fault zone formed at depths of 8–10km may,

depending on the host rock lithology, cyclically evolve from a fluid conduit, through a conduit–barrier, and finally a full fluid barrier.

Implications for passive margin evolution

The ultracataclasites observed in the Rekvika fault zone are suggested to be comparable with ultracataclasites described by Wibberley (1999) and thus reflect early stages of faulting. Their *in situ* presence indicates that the Late Permian–Early Triassic faulting came to a halt during early (deep) stages of faulting, to prevent subsequent formation of phyllosilicates within the fault zone. Thus, the preservation of these ultracataclasites may coincide with, and be a result of, the westward migration of fault activity to offshore fault complexes after Late Permian–Early Triassic (Davids *et al.* 2013; Indrevær *et al.* 2013). Furthermore, an average geothermal gradient for the upper continental crust is in the range of 25–30 °C km⁻¹. Within early stages of continental rifting, both palaeo- and present geothermal gradients tends to be elevated, especially within subsiding rift-basins, and may exceed 50 °C km⁻¹ (Ru & Pigott 1986; Qiu & Wang 1998; Sandiford *et al.* 1998; Liu *et al.* 2001; Wang *et al.* 2011). The geothermal gradient of *c.* 30 °C km⁻¹ calculated in this study suggest either that onshore faulting occurred during early phases of rifting along the SW Barents Sea margin, or that the faulting was located along the rift flanks, where geothermal gradients may have remained relatively unchanged.

An uplift of the coastal part of the SW Barents Sea margin has been suggested as part of the formation of the Scandes Mountains (see Corner 2005). The timing and nature of such uplift(s) have been widely discussed in the literature (see Doré *et al.* 2002). The depth estimates from the studied fault zones are used in conjunction with the Late Permian time constraints on faulting in the region (Davids *et al.* 2013) to calculate a minimum average exhumation rate of *c.* 40 m Ma⁻¹ for the outer islands of Troms since the Late Permian. When we consider that continental average erosion rates typically range from *c.* 10 to 100 m Ma⁻¹ (e.g. Stallard 1988; Schaller *et al.* 2001, 2002; Charreau *et al.* 2011) and that the SW Barents Sea region has experienced extensive glacial erosion in the last 2.7 Ma with an average erosion rate of *c.* 380 m Ma⁻¹ (Laberg *et al.* 2012), the values suggest that erosion alone can explain the regional exhumation since Permian times: the Late Cenozoic tectonic uplift of the margin may be due to climate deterioration after the formation of the North Atlantic Ocean, which caused subsequent isostatic recalibration and greater uplift of the marginal crust owing to a faster rate of erosion along the margin than inland.

In terms of fault permeability and fluid flow, the studied Late Permian–Early Triassic fault zones may have acted as fluid barriers since this rifting phase. If we assume that the permeability of the basement fault rocks onshore is analogous to that of basement-seated faults offshore, then faults such as those present on the proximal shelf along the SW Barents Sea margin (i.e. the Finnmark Platform and the Loppa High) have the potential to act as hydrocarbon traps. In contrast, any later reactivation of faults after the emplacement of hydrocarbons would most probably increase along-fault permeability and allow for migration of hydrocarbons up through the fault zone.

Conclusions

- (1) Late Permian–Early Triassic brittle normal faults make up a network of basement-seated faults that occur both onshore and offshore along the SW Barents Sea passive margin. These faults show varying amounts of displacement from >3 km to hundreds of metres or less, and they comprise distinctive cataclastic fault rocks.
- (2) Minimum P – T conditions during early stages of faulting are estimated to be *c.* 300 °C and *c.* 240 MPa (*c.* 10 km depth) based on greenschist-facies mineral assemblages of the cataclasites. Later fault movement introduced pumpellyite, yielding minimum P – T conditions of *c.* 275 °C and *c.* 220 MPa (*c.* 8.5 km depth).
- (3) The quartzitic ultracataclasites that occur within granitoid fault rocks are interpreted to be preserved fault rocks from early stages of faulting that formed as a result of the chemical breakdown of feldspar to epidote with the release of quartz. Fault activity is interpreted to have come to a halt during early (and deep) stages of rifting, as there is no subsequent formation of phyllosilicates within the process zone.
- (4) Microstructural evidence indicates that pore pressures locally reached lithostatic levels (240 MPa) during faulting. Fluidized cataclasites allowed for the estimation of the minimum fluid velocity necessary, yielding a value on the order of 10^{-1} m s^{-1} .
- (5) The brittle faults within the basement rocks acted as important fluid conduits during rifting in the Late Permian–Early Triassic. A model is proposed, suggesting that fluid flow was concentrated in the core zone during faulting and in the damage zone during periods after faulting. Healing and precipitation processes probably sealed off the fault zones within a short time span after faulting.

(6) A maximum geothermal gradient during faulting in the Late Permian–Early Triassic of *c.* 30 °C km⁻¹ is calculated based on the occurrence of pumpellyite. The un-elevated geothermal gradient suggests either that faulting occurred during early stages of continental rifting or that the studied fault zones were located along the rift flanks where little to no subsidence took place.

(7) A minimum average exhumation rate of *c.* 40 m Ma⁻¹ since the Late Permian is estimated for the West Troms Basement Complex. When considering normal erosion rates, the proposed late Cenozoic uplift, which has been discussed widely in the literature, may be explained by climate deterioration after the formation of the North Atlantic Ocean, causing subsequent isostatic crustal recalibration and greater isostatic uplift of the margin crust owing to a greater amount of erosion along the margin than inland.

(8) As the studied fault zones are the onshore portions of large fault complexes that continue offshore, it is likely that the studied fault zones are analogous to basement-seated faults offshore. This implies that the conditions and nature of faulting observed onshore may be valid for offshore faults, including past and present fault zone permeability and potential for hydrocarbon entrapment.

Acknowledgements: This work was part of the Industrial PhD scheme organized by the Norwegian Research Council. The project is a collaboration between DONG E&P Norge and the University of Tromsø, financed by DONG E&P Norge and the Norwegian Research Council. We would like to express our gratitude to all those involved from these institutions.

References

- Antonsdóttir, V. 2006. *Structural and kinematic analysis of the post-Caledonian Rekvika Fault Zone, Kvaløya, Troms*. Unpublished Master thesis, University of Tromsø, 84 pp.
- Bergh, S. G., Eig, K., Kløvjan, O. S., Henningsen, T., Olesen, O. & Hansen, J-A. 2007. The Lofoten-Vesteralen continental margin: a multiphase Mesozoic-Palaeogene rifted shelf as shown by offshore-onshore brittle fault-fracture analysis. *Norwegian Journal of Geology*, v. **87**, 29 - 58.
- Bergh, S. G., Kullerud, K., Armitage, P. E. B., Zwaan, K. B., Corfu, F., Ravna, E. J. K. & Myhre, P. I. 2010. Neoproterozoic through Svecofennian tectono-magmatic evolution of the West Troms Basement Complex, North Norway. *Norwegian Journal of Geology*, v. **90**, 21-48.
- Blanpied, M. L., Lockner, D. A. & Byerlee, J. D. 1992. An earthquake mechanism based on rapid sealing of faults. *Nature*, **358**(6387), 574-576.
- Blystad, P., Brekke, H., Færseth, R. B., Larsen, B. T., Skogseid, J. & Tørudbakken, B. 1995: Structural elements of the Norwegian continental shelf, Part II. The Norwegian Sea Region. *Norwegian Petroleum Directorate Bulletin*, v. 8. 45pp.

- Boone, G. M. 1969. Origin of clouded red feldspars; petrologic contrasts in a granitic porphyry intrusion. *American Journal of Science*, **267**(6), 633-668.
- Bos, B. & Spiers, C. J. 2000. Effect of phyllosilicates on fluid-assisted healing of gouge-bearing faults. *Earth and Planetary Science Letters*, **184**(1), 199-210.
- Brace, W. F. & Kohlstedt, D. L. 1980. Limits on lithospheric stress imposed by laboratory experiments. *Journal of Geophysical Research. Solid Earth (1978–2012)*, **85**(B11), 6248-6252.
- Bruhn, R. L., Parry, W. T., Yonkee, W. A. & Thompson, T. 1994. Fracturing and hydrothermal alteration in normal fault zones. *Pure and Applied Geophysics*, **142**(3-4), 609-644.
- Bucher, K. & Grapes, R. H. 2011. *Petrogenesis of metamorphic rocks*. Springer.
- Byerlee, J. 1978. Friction of rocks. *Pure and applied Geophysics*, **116**(4-5), 615-626.
- Byerlee, J. 1990. Friction, overpressure and fault normal compression. *Geophysical Research Letters*, **17**(12), 2109-2112.
- Byerlee, J. D. 1993. Model for episodic flow of high-pressure water in fault zones before earthquakes. *Geology*, **21**(4), 303-306.
- Caine, J. S., Evans, J. P. & Forster, C. B. 1996. Fault zone architecture and permeability structure. *Geology*, **24**(11), 1025-1028.
- Caine, J. S., Bruhn, R. L. & Forster, C. B. 2010. Internal structure, fault rocks, and inferences regarding deformation, fluid flow, and mineralization in the seismogenic Stillwater normal fault, Dixie Valley, Nevada. *Journal of Structural Geology*, **32**(11), 1576-1589.
- Charreau, J., Blard, P. H., Puchol, N., Avouac, J. P., Lallier-Vergès, E., Bourlès, D., ... & Roy, P. 2011. Paleo-erosion rates in Central Asia since 9Ma: A transient increase at the onset of Quaternary glaciations? *Earth and Planetary Science Letters*, **304**(1), 85-92.
- Corfu, F. 2004. U–Pb age, setting and tectonic significance of the anorthosite–mangerite–charnockite–granite suite, Lofoten–Vesterålen, Norway. *Journal of Petrology*, **45**(9), 1799-1819.
- Corfu, F., Armitage, P. E. B., Kullerud, K. & Bergh, S. G. 2003. Preliminary U-Pb geochronology in the West Troms Basement Complex North Norway: Archaean and Palaeoproterozoic events and younger overprints. *Geological Survey of Norway, Bulletin* **441**, 61-72.
- Corner, G. D. 2005. Chap 12. Atlantic coast and fjords. In: Seppälä, M. (ed.). *The physical Geography of Fennoscandia, Oxford Regional Environments Series*, Oxford University Press, 203-228.
- Crampin, S., Gudmundsson, A. & Stefánsson, R. 2002. Indication of high pore-fluid pressures in a seismically-active fault zone. *Geophysical Journal International*, **151**(2), F1-F5.
- Dalland, A. 1981. Mesozoic sedimentary succession at Andøya, Northern Norway, and relation to structural development of the North Atlantic area. In: Kerr, J. W. & Fergusson, A. J. (eds.) *Geology of the North Atlantic borderlands. Canadian Society of Petroleum Geologists, Memoir* **7**, 563-584.
- Davids, C., Wemmer, K., Zwingmann, H., Kohlmann, F., Jacobs, J. & Bergh, S. G. 2013. K–Ar illite and apatite fission track constraints on brittle faulting and the evolution of the northern Norwegian passive margin. *Tectonophysics*, **608**, 196-211.
- Delaney, P. T., Pollard, D. D., Ziony, J. I. & McKee, E. H. 1986. Field relations between dikes and joints: Emplacement processes and paleostress analysis. *Journal of Geophysical Research* **91**, p. 4920-4938.
- Doré, A. G., Lundin, E. R., Fichler, C. & Olesen, O. 1997. Patterns of basement structure and reactivation along the NE Atlantic margin. *Journal of the Geological Society of London* **154**, 85-92
- Doré, A. G., Lundin, E. R., Jensen, L. N., Birkeland, Ø., Eliassen, P. E. & Fichler, C. 1999. Principal tectonic events in the evolution of the northwest European Atlantic margins. In: Fleet, A. J. & Boldy,

- S. A. R. (eds.), *Petroleum Geology of Northwest Europe: Proceedings of the 5th Conference. Geological Society of London*, 41-61.
- Doré, A. G., Cartwright, J. A., Stoker, M. S., Turner, J. P. & White, N. (eds.) 2002. Exhumation of the North Atlantic Margin: Timing, Mechanisms and Implications for Petroleum Exploration, *Special Publications - Geological Society of London*, v. **196**, 45-65.
- Drake, H., Tullborg, E. L. & Annersten, H. 2008. Red-staining of the wall rock and its influence on the reducing capacity around water conducting fractures. *Applied Geochemistry*, **23**(7), 1898-1920.
- Eichhubl, P. & Boles, J. R., 2000. Rates of fluid flow in fault systems; evidence for episodic rapid fluid flow in the Miocene Monterey Formation, coastal California. *American Journal of Science*, **300**(7), 571-600.
- Eig, K. 2008. *Onshore and offshore tectonic evolution of the Lofoten passive margin, North Norway*. Unpublished PhD thesis, University of Tromsø, 256 pp.
- Faulkner, D. R., Jackson, C. A. L., Lunn, R. J., Schlische, R. W., Shipton, Z. K., Wibberley, C. A. J. & Withjack, M. O. 2010. A review of recent developments concerning the structure, mechanics and fluid flow properties of fault zones. *Journal of Structural Geology*, **32**(11), 1557-1575.
- Faleide, J. I., Tsikalas, F., Breivik, A. J., Mjelde, R., Ritzmann, O., Engen, O., Wilson, J. & Eldholm, O. 2008. Structure and evolution of the continental margin off Norway and Barents Sea. *Episodes* **31**(1), 82-91.
- Forslund, T. 1988. *Post-Kaledonske forkastninger i Vest-Troms, med vekt på Kvaløyslettaforkastningen, Kvaløya*. Unpublished Cand. Scient. thesis, University of Tromsø. 173 pp.
- Fürsich, F. & Thomsen, E. 2005. Jurassic biota and biofacies in erratics from the Sortland area, Vesterålen, northern Norway. *Geological Society of Norway, Bulletin* **443**, 37-53.
- Gabrielsen, R.H., Færseth, R.B., Jensen, L.N., Kalheim, J.E. & Riis, F. 1990. Structural elements of the Norwegian continental shelf — Part I: the Barents Sea Region. *Norwegian Petroleum Directorate Bulletin* **6**, 33 pp.
- Ganerød, G. V., Braathen, A., & Willemoes-Wissing, B. 2008. Predictive permeability model of extensional faults in crystalline and metamorphic rocks; verification by pre-grouting in two sub-sea tunnels, Norway. *Journal of Structural Geology*, **30**(8), 993-1004.
- Gernigon, L. & Brönnner, M. 2012. Late Palaeozoic architecture and evolution of the southwestern Barents Sea: insights from a new generation of aeromagnetic data. *Journal of the Geological Society*, **169**(4), 449-459.
- Goodman, R. E. 1989. *Introduction to rock mechanics*, 2nd edn. Wiley, New York.
- Gudmundsson, A., Berg, S. S., Lyslo, K. B. & Skurtveit, E. 2001. Fracture networks and fluid transport in active fault zones. *Journal of Structural Geology*, **23**(2), 343-353.
- Haimson, B. & Fairhurst, C. 1967. Initiation and extension of hydraulic fractures in rocks. *SPE Journal*, **7**(3), 310-318.
- Hansen, J.-A. 2009. *Onshore-offshore tectonic relations on the Lofoten and Vesterålen Margin - Mesozoic to early Cenozoic structural evolution and morphological implications*. PhD thesis, University of Tromsø, 229 pp.
- Hansen, J. A., Bergh, S. G., & Henningsen, T. 2012: Mesozoic rifting and basin evolution on the Lofoten and Vesterålen Margin, North-Norway; time constraints and regional implications. *Norwegian Journal of Geology*, **91**, 203-228.
- Hendriks, B. W. H., Osmundsen, P. T. & Redfield, T. F. 2010. Normal faulting and block tilting in Lofoten and Vesterålen constrained by apatite fission track data. *Tectonophysics* **485**, 154-163.

- Hickman, S., Sibson, R. & Bruhn, R. 1995. Introduction to special section: Mechanical involvement of fluids in faulting. *Journal of Geophysical Research: Solid Earth (1978–2012)*, **100**(B7), 12831-12840.
- Holdsworth, R. E. 2004: Weak Faults - Rotten Cores. *Science*, *303*(5655), 181-182.
- Hubbert, M. K. & Rubey, W. W. 1959. Role of fluid pressure in mechanics of overthrust faulting I. Mechanics of fluid-filled porous solids and its application to overthrust faulting. *Geological Society of America Bulletin*, **70**(2), 115-166.
- Indrevær, K., Bergh, S.G., Koehl, J-B, Hansen, J-A, Schermer, E., & Ingebrigtsen, A., 2013. Post-Caledonian brittle fault zones on the hyper-extended SW Barents Sea Margin: New insights into onshore and offshore margin architecture. *Norwegian Journal of Geology*, Vol. 93, pp. 167–188. Trondheim 2013, ISSN 029-196X.
- Jaeger, J. C., Cook, N. G. & Zimmerman, R. 2009. *Fundamentals of rock mechanics*. Wiley. com.
- Janecke, S. U., & Evans, J. P. 1988. Feldspar-influenced rock rheologies. *Geology*, *16*(12), 1064-1067.
- Jefferies, S. P., Holdsworth, R. E., Wibberley, C. A. J., Shimamoto, T., Spiers, C. J., Niemeijer, A. R., & Lloyd, G. E. 2006. The nature and importance of phyllonite development in crustal-scale fault cores: an example from the Median Tectonic Line, Japan. *Journal of Structural Geology*, *28*(2), 220-235.
- Kanagawa, K., Cox, S. F. & Zhang, S. 2000. Effects of dissolution-precipitation processes on the strength and mechanical behavior of quartz gouge at high-temperature hydrothermal conditions. *Journal of Geophysical Research: Solid Earth (1978–2012)*, **105**(B5), 11115-11126.
- Karner, S. L., Marone, C. & Evans, B. 1997. Laboratory study of fault healing and lithification in simulated fault gouge under hydrothermal conditions. *Tectonophysics*, **277**(1), 41-55.
- Keulen, N., Stünitz, H. & Heilbronner, R. 2008. Healing microstructures of experimental and natural fault gouge. *Journal of Geophysical Research: Solid Earth (1978–2012)*, **113**(B6). DOI: 10.1029/2007JB005039
- Laberg, J. S., Andreassen, K. & Vorren, T. O. 2012. Late Cenozoic erosion of the high-latitude southwestern Barents Sea shelf revisited. *Geological Society of America Bulletin*, **124**(1-2), 77-88.
- Mosar, J., Torsvik, T. H. & the BAT team 2002. Opening the Norwegian and Greenland Seas: Plate tectonics in Mid Norway since the Late Permian. In: Eide, E.A. (coord.), *BATLAS - Mid Norway plate reconstruction atlas with global Atlantic perspectives*, 48-59. The Geological Survey of Norway, Trondheim.
- Nakano, S., Akai, J. & Shimobayashi, N. 2005. Contrasting Fe-Ca distributions and related microtextures in syenite alkali feldspar from the Patagonian Andes, Chile. *Mineralogical Magazine*, **69**(4), 521-535.
- Nakatani, M. & Scholz, C. H. 2004. Frictional healing of quartz gouge under hydrothermal conditions: 1. Experimental evidence for solution transfer healing mechanism. *Journal of Geophysical Research: Solid Earth (1978–2012)*, **109**(B7). DOI: 10.1029/2001JB001522
- Nansheng, Q. & Jiyang, W. 1998. The use of free radicals of organic matter to determine paleogeothermal gradient. *Organic geochemistry*, **28**(1-2), 77-86.
- Olesen, O., Torsvik, T. H., Tveten, E., Zwaan, K. B., Løseth, H. & Henningsen, T. 1997. Basement structure of the continental margin in the Lofoten-Lopphavet area, northern Norway: constraints from potential field data, on-land structural mapping and palaeomagnetic data, *Norwegian Journal of Geology* **77**, 15–30.
- Olsen, M. P., Scholz, C. H. & Léger, A. 1998. Healing and sealing of a simulated fault gouge under hydrothermal conditions: Implications for fault healing. *Journal of Geophysical Research: Solid Earth (1978–2012)*, **103**(B4), 7421-7430.

- Opheim, J.A. and Andresen, A. 1989. Basement-cover relationships on northern Vanna, Troms, Norway. *Norwegian Journal of Geology*, v. **69**(2), 67-81.
- Osmundsen, P. T., Redfield, T. F., Hendriks, B. H. W., Bergh, S., Hansen, J. A., Henderson, I. H. C., Dehls, J., Lauknes, T.R., Larsen, Y., Anda, E. & Davidsen, B. 2010: Fault-controlled alpine topography in Norway. *Journal of the Geological Society*, **167**(1), 83-98.
- Putnis, A., Hinrichs, R., Putnis, C. V., Golla-Schindler, U. & Collins, L. G. 2007. Hematite in porous red-clouded feldspars: evidence of large-scale crustal fluid-rock interaction. *Lithos*, **95**(1), 10-18.
- Rice, J. R. 1992. Fault stress states, pore pressure distributions, and the weakness of the San Andreas fault. *International Geophysics Series*, **51**, p. 475-503.
- Roberts, D. & Lippard, S.J. 2005. Inferred Mesozoic faulting in Finnmark: current status and offshore links. *Geological Survey of Norway Bulletin* **443**, 55-60.
- Rodrigues, N., Cobbold, P. R. & Løseth, H. 2009. Physical modelling of sand injectites. *Tectonophysics*, **474**(3), 610-632.
- Ru, K. & Pigott, J. D. 1986. Episodic rifting and subsidence in the South China Sea. *Am. Assoc. Pet. Geol., Bull.:(United States)*, **70**(9).
- Rutter, E. H., Holdsworth, R. E., & Knipe, R. J. 2001: The nature and tectonic significance of fault-zone weakening: an introduction. *Geological Society, London, Special Publications*, **186**(1), 1-11.
- Sandiford, M., Hand, M. & McLaren, S. 1998. High geothermal gradient metamorphism during thermal subsidence. *Earth and Planetary Science Letters*, **163**(1), 149-165.
- Schaller, M., von Blanckenburg, F., Hovius, N. & Kubik, P. W. 2001. Paleo-Erosion Rates From in Situ ¹⁰Be in Middle European River Terrace Sediments. In *AGU Fall Meeting Abstracts* (Vol. **1**, p. 0449).
- Schaller, M., Von Blanckenburg, F., Veldkamp, A., Tebbens, L. A., Hovius, N. & Kubik, P. W. 2002: A 30 000 yr record of erosion rates from cosmogenic ¹⁰Be in middle European river terraces. *Earth and Planetary Science Letters*, **204**(1), 307-320.
- Schmidt, E. H. W. and F. Mayinger, 1963. Viscosity of Water and Steam at High Pressures and Temperatures Up to 800 Atmospheres and 700 C. Edited by Warren Ibele. *Modern Developments in Heat Transfer*, p. 265-278. Academic Press Inc, New York.
- Seront, B., Wong, T. F., Caine, J. S., Forster, C. B., Bruhn, R. L. & Fredrich, J. T. 1998. Laboratory characterization of hydromechanical properties of a seismogenic normal fault system. *Journal of structural geology*, **20**(7), 865-881.
- Sibson, R. H. 1973. Frictional constraints on thrust, wrench and normal faults. *Nature*, **249**, 542-544.
- Sibson, R. H. 1977. Fault rocks and fault mechanisms. *Journal of the Geological Society*, **133**(3), 191-213.
- Sibson, R. H. 1989. Earthquake faulting as a structural process. *Journal of Structural Geology*, **11**(1), 1-14.
- Sibson, R. H., Moore, J. M. M. & Rankin, A. H. 1975. Seismic pumping—a hydrothermal fluid transport mechanism. *Journal of the Geological Society*, **131**(6), 653-659.
- Smelror, M., Petrov, O.V., Larsen, G.B. & Werner, S.C. (eds.) + 16 co-authors 2009. *Geological history of the Barents Sea*. Geological Survey of Norway, Trondheim, 135 pp.
- Smith, J. V. & Brown, W. L. 1988. *Feldspar minerals*. Springer-Verlag.
- Stallard, R. F. 1988. Weathering and erosion in the humid tropics. In *Physical and Chemical Weathering in Geochemical Cycles* (pp. 225-246). Eds: Lerman, A. & Meybeck, M. Springer Netherlands.

- Taylor, H. P. 1977. Water/rock interactions and the origin of H₂O in granitic batholiths Thirtieth William Smith lecture. *Journal of the Geological Society*, **133**(6), 509-558.
- Tegner, C. 1997. Iron in plagioclase as a monitor of the differentiation of the Skaergaard intrusion. *Contributions to Mineralogy and Petrology*, **128**(1), 45-51.
- Thorstensen, L. 2011. *Land-sokkel korrelasjon av tektoniske elementer i ytre del av Senja og Kvaløya i Troms*. Unpublished Master thesis, University of Tromsø, 107 pp.
- Torgersen, E., Viola, G. & Zwingmann, H. 2013. How can K-Ar geochronology of clay-size mica/illite help constrain reactivation histories of brittle faults? An example from a Paleozoic thrust fault in Northern Norway. In EGU General Assembly Conference Abstracts (Vol. 15, p. 2986).
- Wang, W., Zhou, Z., Guo, T. & Xu, C. 2011. Early cretaceous-paleocene geothermal gradients and Cenozoic tectono-thermal history of Sichuan basin. *Journal of Tongji University. Natural Science*, **39**(4), 606-613.
- Wibberley, C. 1999. Are feldspar-to-mica reactions necessarily reaction-softening processes in fault zones?. *Journal of Structural Geology*, **21**(8), 1219-1227.
- Wintsch, R. P., Christoffersen, R., & Kronenberg, A. K. 1995. Fluid-rock reaction weakening of fault zones. *Journal of Geophysical Research: Solid Earth (1978–2012)*, **100**(B7), 13021-13032.
- Yiqun, L., Mingsheng, Y., Dingwu, Z., Qiao, F. & Jun, J. 2001. New progresses on geothermal history of Turpan-Hami Basin, Xinjiang, China. *Science in China Series D: Earth Sciences*, **44**(2), 166-176.
- Zoback, M. D. 1991. State of stress and crustal deformation along weak transform faults. *Philosophical Transactions of the Royal Society of London. Series A: Physical and Engineering Sciences*, **337**(1645), 141-150.
- Zoback, M. D. & Townend, J. 2001. Implications of hydrostatic pore pressures and high crustal strength for the deformation of intraplate lithosphere. *Tectonophysics*, **336**(1), 19-30.
- Zwaan, K. B. 1995. Geology of the West Troms Basement Complex, northern Norway, with emphasis on the Senja Shear Belt: a preliminary account. *Geological Survey of Norway, Bulletin* **427**, 33-36.

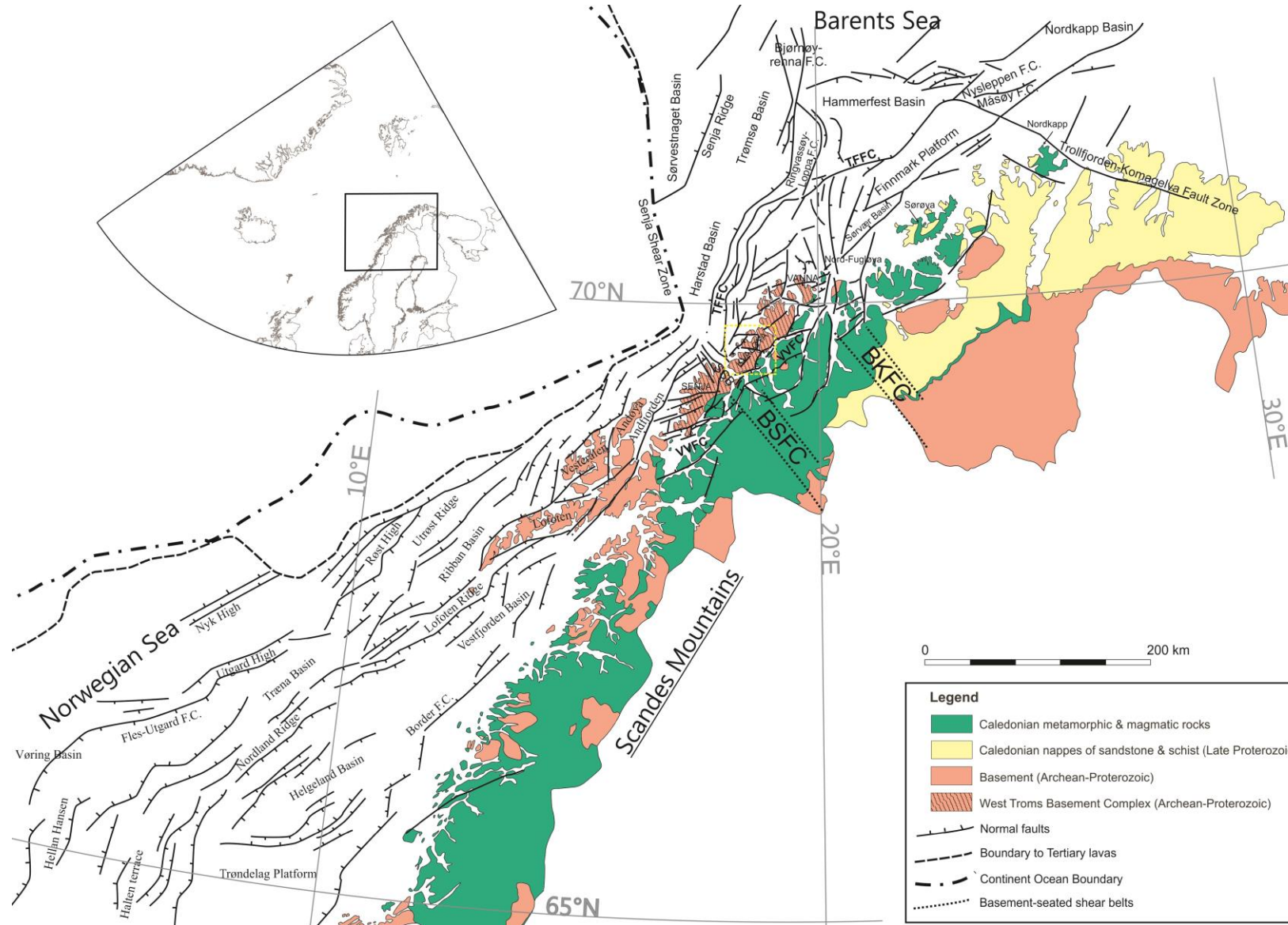


Fig. 1. Regional onshore–offshore tectonic map and setting of the mid-Norwegian shelf, the West Troms Basement Complex and the SW Barents Sea margin (after Blystad *et al.* 1995; Mosar *et al.* 2002; Bergh *et al.* 2007; Faleide *et al.* 2008; Hansen *et al.* 2012; Indrevær *et al.* 2014). Onshore geology is from the Geological Survey of Norway. The yellow box outlines Figure 2. BKFC, Bothnian-Kvænangen Fault Complex; BSFC, Bothnian-Senja Fault Complex; TFFC, Troms–Finmark Fault Complex; VVFC, Vestfjorden–Vanna Fault Complex.

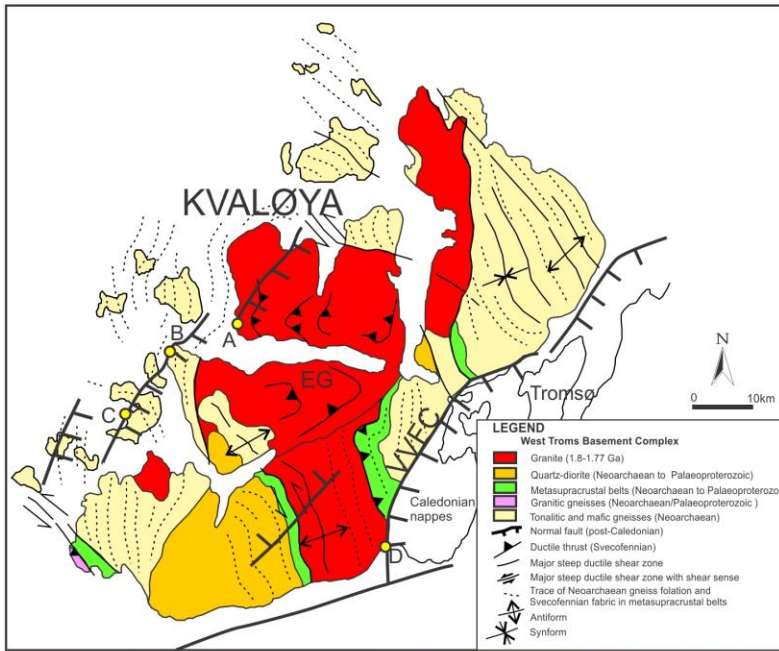
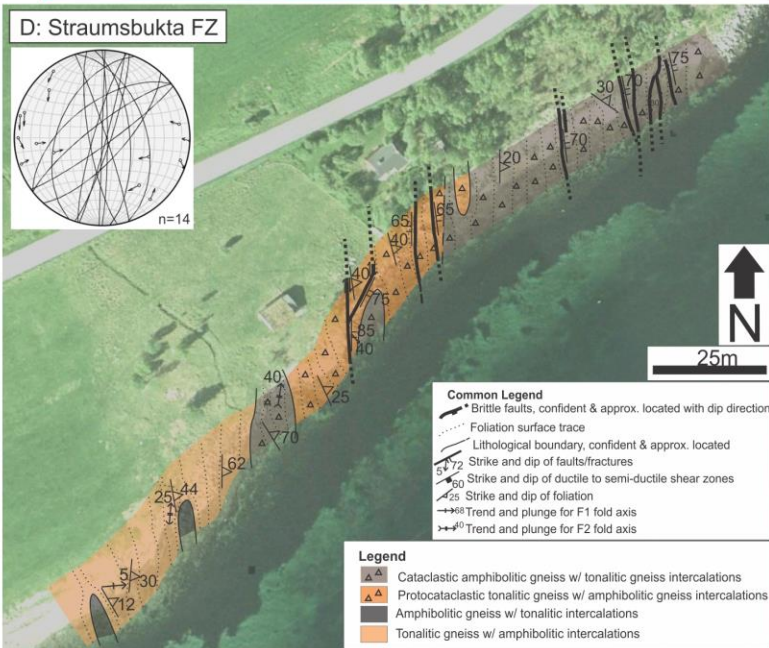
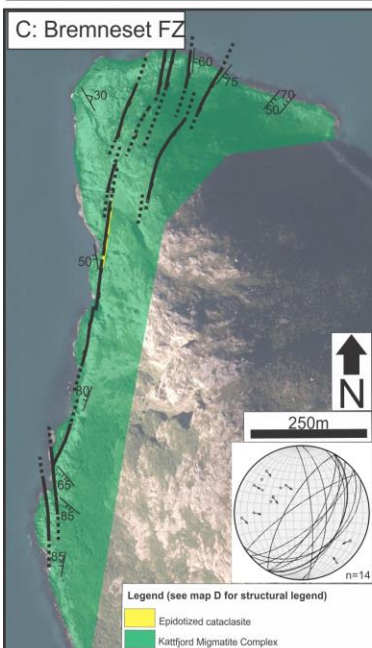
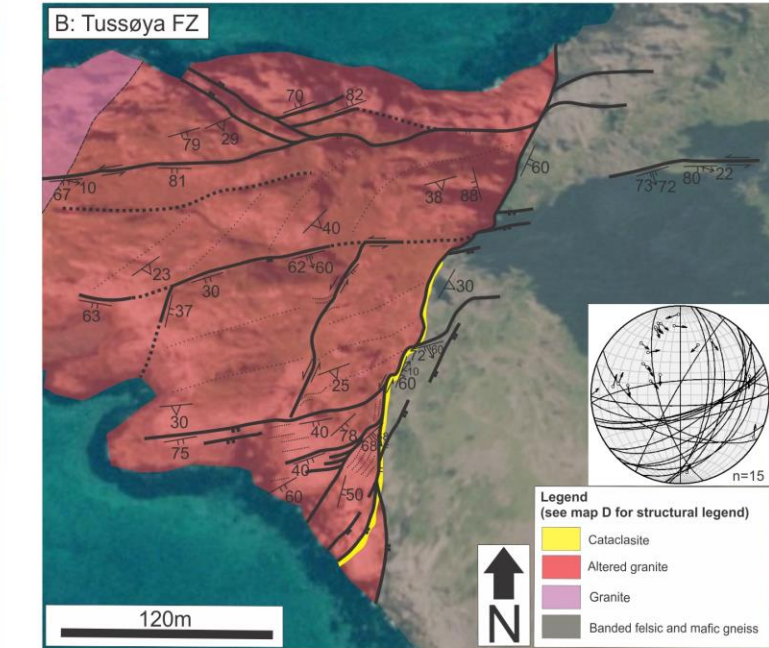
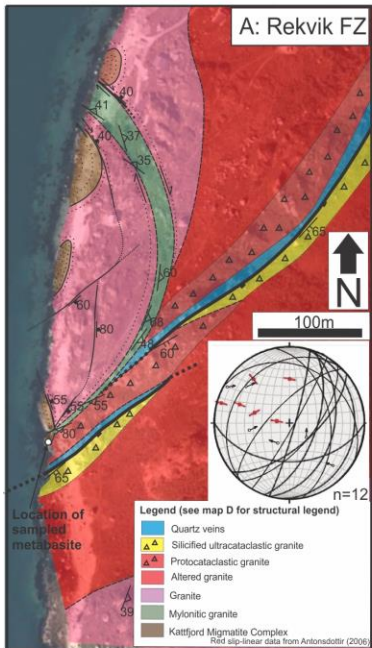


Fig. 2. Geological map of the Kvaløya area with the location of the studied fault outcrops marked A–D. Detailed structural maps from the studied fault zones are presented in the inset maps A–D (after Indrevær *et al.* 2013). Fault orientation data are plotted as great circles and poles to planes with direction of slip-linear data for the hanging wall in lower hemisphere equal-area stereonet. EG, Ersfjord Granite; VVFC, Vestfjorden–Vanna Fault Complex.



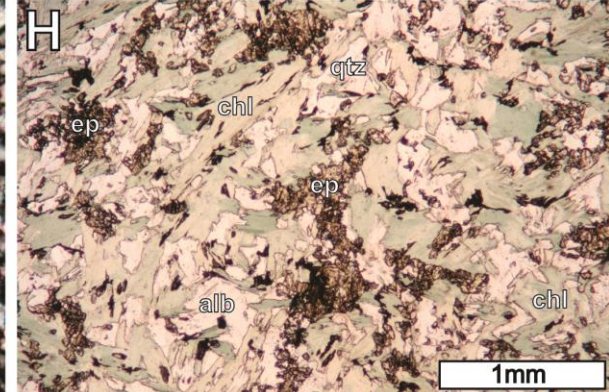
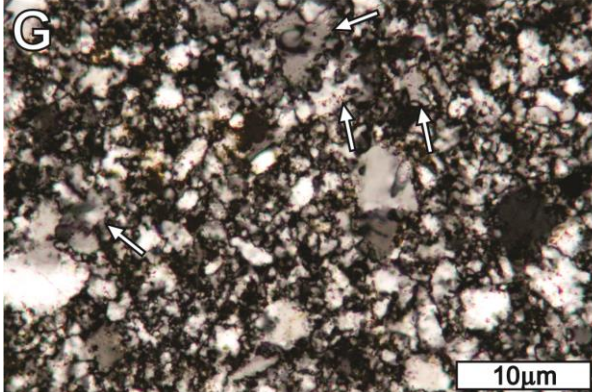
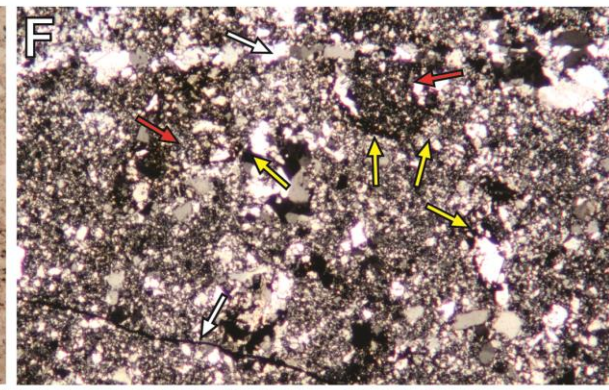
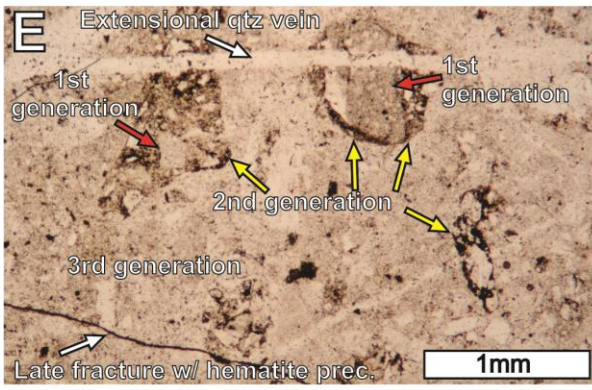
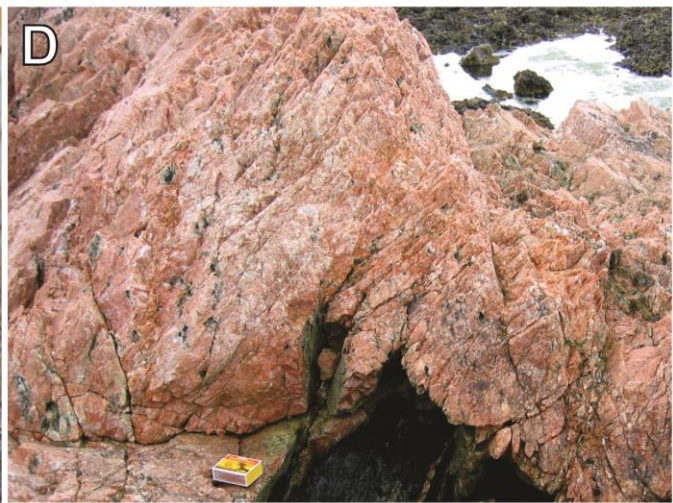
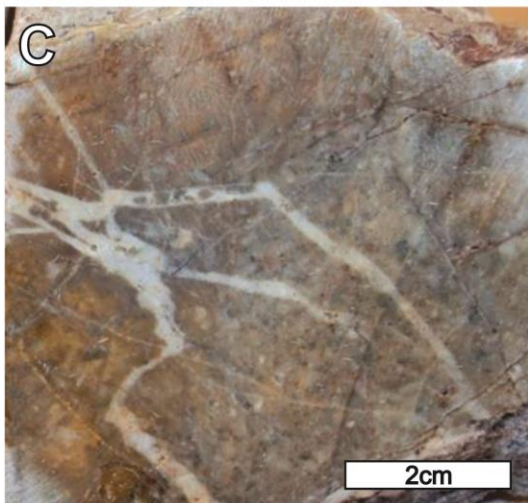
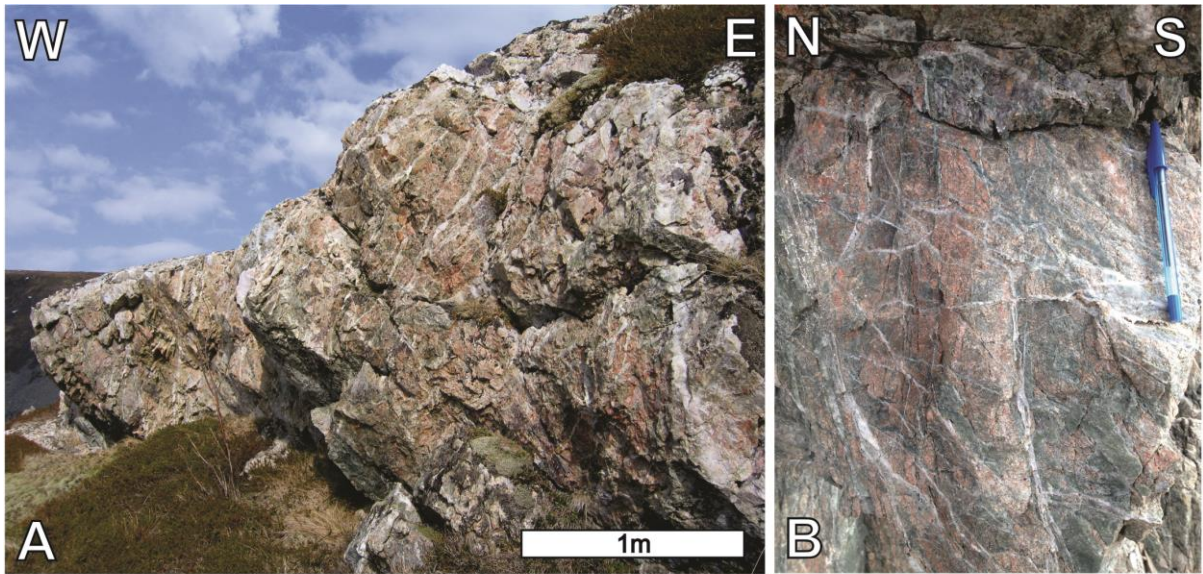
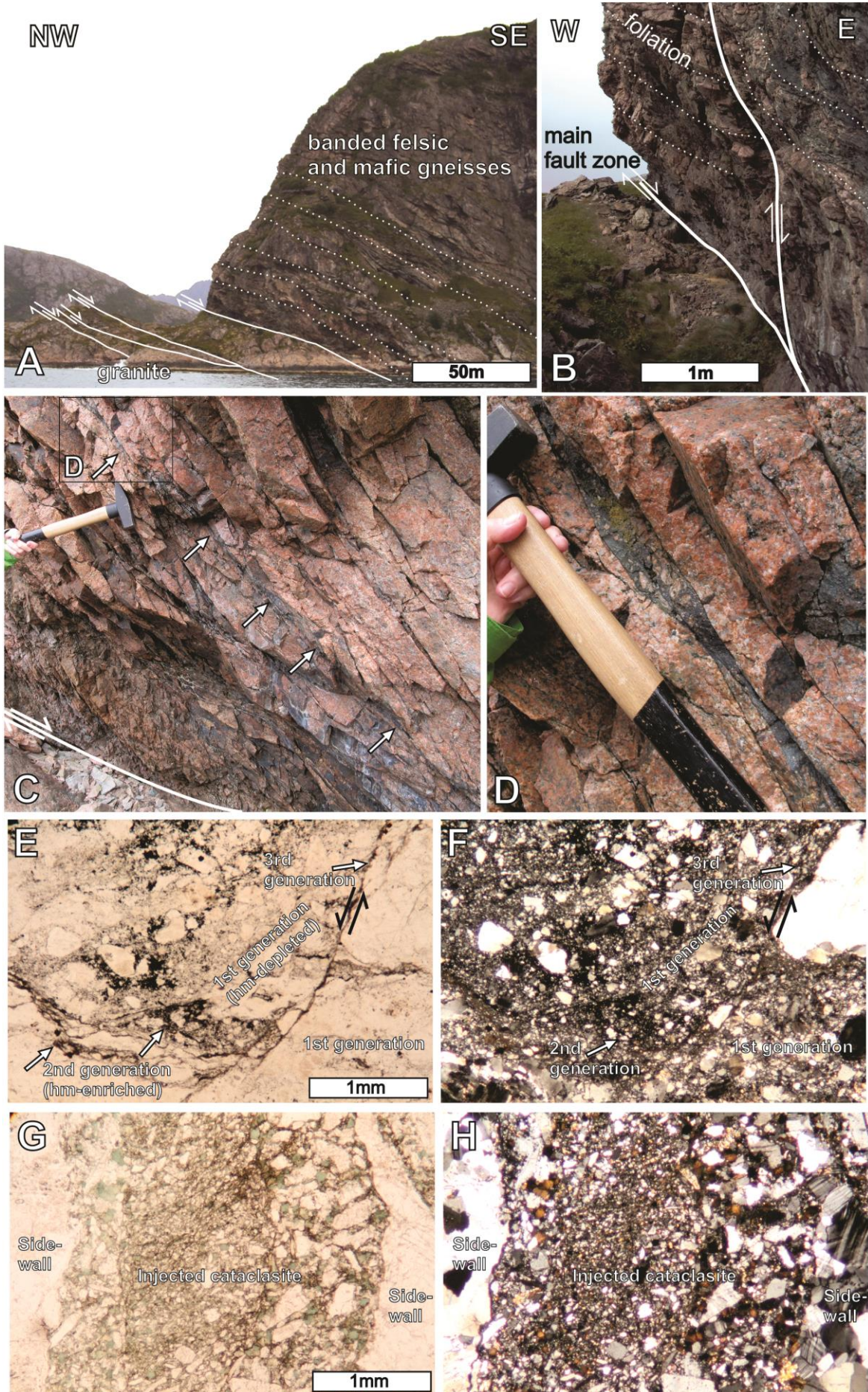


Fig. 3. (Previous page) Outcrop photographs and photomicrographs from the Rekvik fault zone. **(a)** Damage zone of the Rekvika fault zone. The extensive occurrence of quartz veins should be noted. **(b)** Close-up of the damage zone close to the process zone. The occurrence of epidote, irregular quartz veins and clasts of red granite should be noted. **(c)** Close-up of quartzitic ultracataclasite from the process zone of the Rekvika fault zone. **(d)** A typical example of red stained granite from the damage zone surrounding the Rekvika fault zone. **(e)** Quartz-rich cataclasite matrix with fragments of former cataclasite cut by extensional quartz veins and late-stage fractures with precipitation of hematite; plane-polarized light. The three generations of cataclasites should be noted. Red arrows indicate first generation; yellow arrows indicate second generation cataclasites. The two first generations are embedded within the matrix of the third generation. **(f)** Same as **(e)** but with crossed polars. **(g)** Indications of grain growth within the fine-grained domain of the second generation of cataclasite in **(e)** and **(f)**; crossed polars. **(h)** A statically recrystallized mafic cataclasite showing a typical greenschist-facies mineral assemblage. alb, albite; chl, chlorite; ep, epidote; qtz, quartz.

Fig. 4. (next page) Outcrop photographs and photomicrographs from the Tussøya fault zone. **(a)** Overview of the fault zone showing how the fault zone separates banded gneisses in the hanging wall from granite in the footwall. **(b)** Detailed photograph of the main fault zone and the hanging wall, indicating the spatial relationship between the main fault zone, subsidiary faults and the gneiss foliation. **(c)** Outcrop photograph of a fault segment from the Tussøya fault zone that cuts through granite. (Note the dark band of ultracataclasite that fills fault-related fractures that are at a high angle to the main fault zone (arrows).) **(d)** Close-up of a dark band of ultracataclasite within the granite host rock. Location is shown in **(c)**. (Note how the cataclasite lacks any internal foliation consistent with high strain and the relatively undamaged sidewalls.) **(e)** Fault rock containing three generations of cataclasites, shown by cross-cutting relationships. **(f)** Same as **(e)** but with crossed

polars. (g) Microfracture composed of injected cataclasite. (h) Same as (g) but with crossed polars.



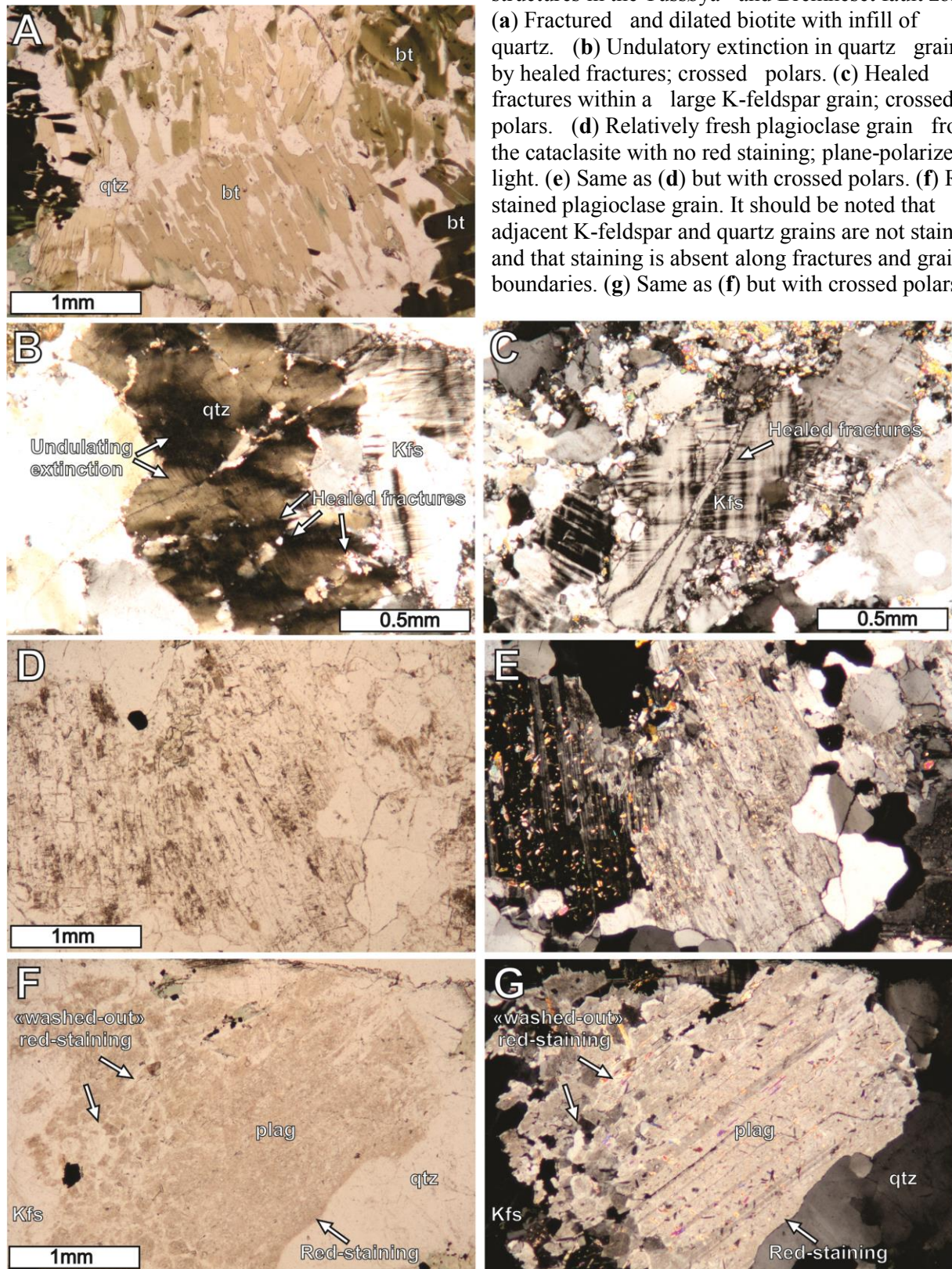


Fig. 5. Photomicrographs of observed deformation structures in the Tussøya and Bremneset fault zones. (a) Fractured and dilated biotite with infill of quartz. (b) Undulatory extinction in quartz grains cut by healed fractures; crossed polars. (c) Healed fractures within a large K-feldspar grain; crossed polars. (d) Relatively fresh plagioclase grain from the cataclasite with no red staining; plane-polarized light. (e) Same as (d) but with crossed polars. (f) Red stained plagioclase grain. It should be noted that adjacent K-feldspar and quartz grains are not stained and that staining is absent along fractures and grain boundaries. (g) Same as (f) but with crossed polars.

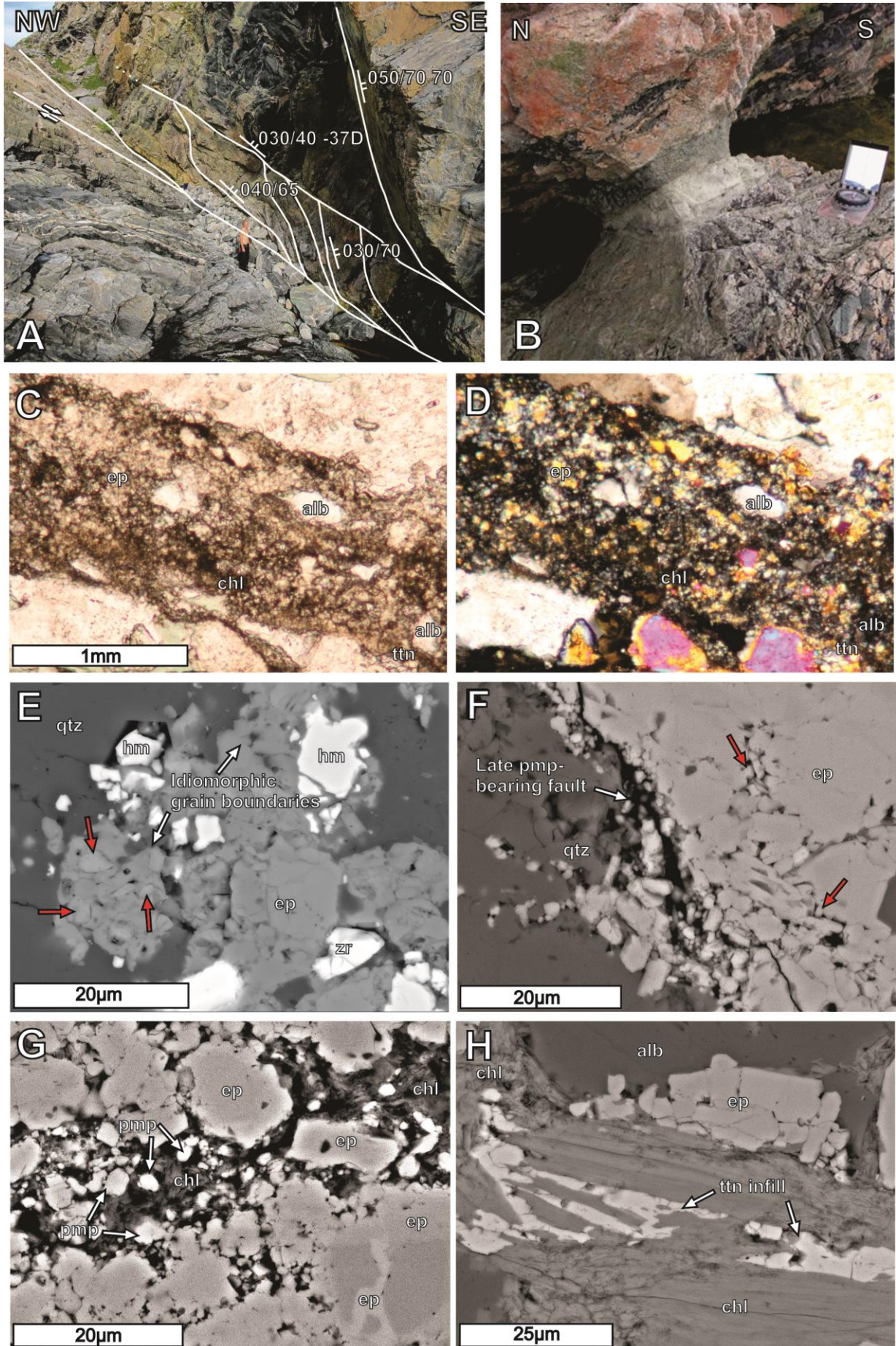


Fig. 6. (previous page) Outcrop photographs, photomicrographs and BSD images of fault rocks from Bremneset. **(a)** Overview of parts of the Bremneset fault zone. (See person for scale.) **(b)** Close-up of a portion of the Bremneset fault zone. The red stained block of granite in the hanging wall should be noted. **(c)** Cataclastic mafic gneiss from the Bremneset fault zone composed of grains with greenschist-facies minerals. **(d)** Same view as **(c)** but with crossed polars. **(e)** BSD image illustrating how clasts of epidote (red arrows) have grown and developed idiomorphic grain boundaries, supporting that greenschist-facies conditions prevailed prior to, during and after early stages of faulting (from Tussøya fault zone). **(f, g)** Idiomorphic epidote grains cut by late-stage microfaults with the formation of pumpellyite (from Bremneset fault zone). The red arrows in **(f)** show examples of preserved epidote clasts from the earlier greenschist-facies fault activity. **(h)** BSD image of fractured and dilated chlorite with titanite infill (from Bremneset fault zone). alb, albite; chl, chlorite; ep, epidote; hm, hematite; ttn, titanite; qtz, quartz; zr, zircon.

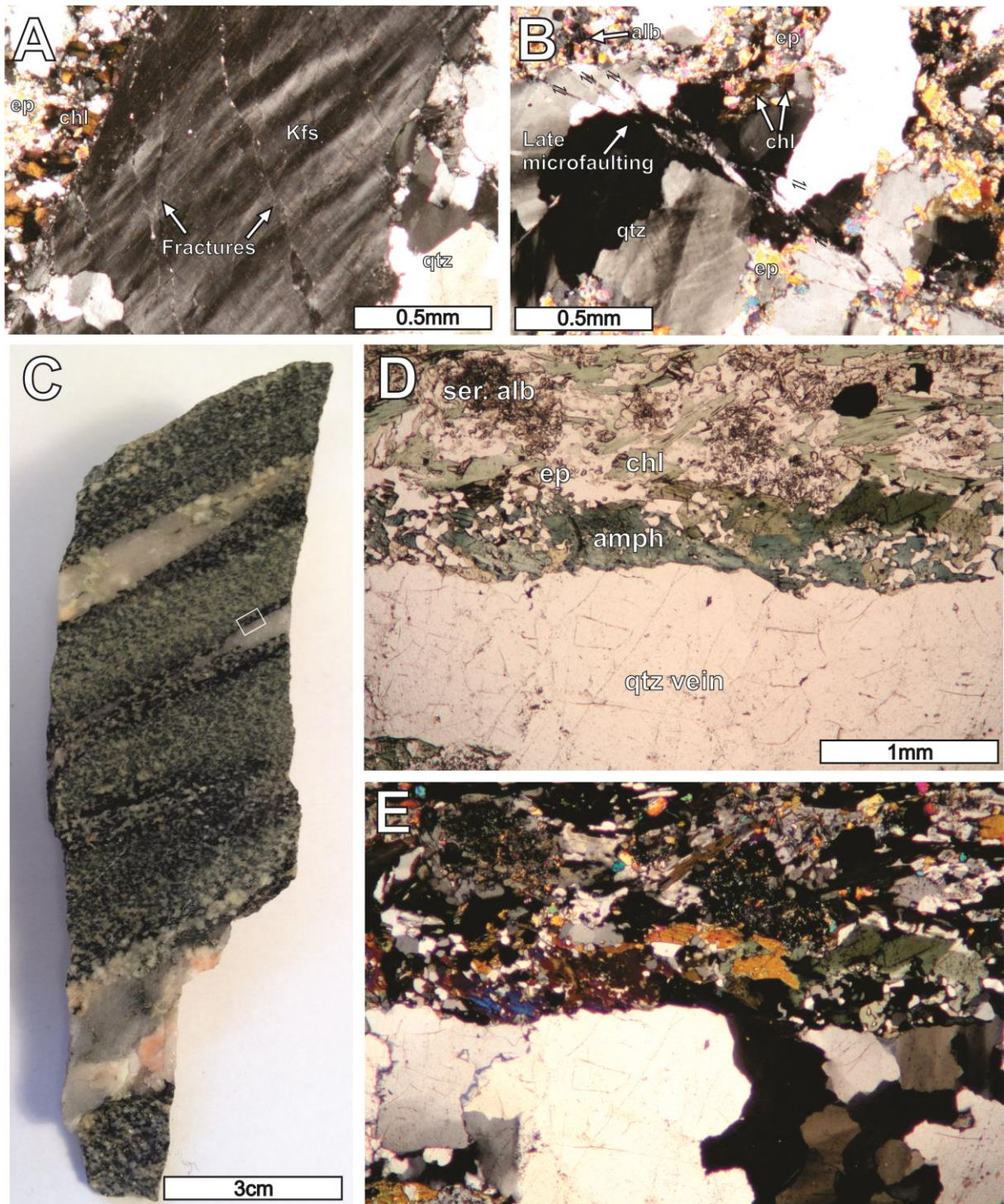


Fig. 7. Photomicrographs and hand-specimen photograph from the Bremneset fault zone. (a, b) Late microfaulting with no development of cataclasite. Crossed polars. (c) Hand-specimen of banded and retrograded amphibolite gneiss with foliation-parallel quartz veins. The preserved zone of amphibolite-facies mineral assemblage (dark bands) along quartz veins that are parallel to ductile foliation and predate the brittle deformation should be noted. Away from the quartz veins, the mafic gneiss is statically retrograded to a greenschist-facies mineral assemblage (green bands). (d) Micrograph showing the zone of preserved amphibole along the rim of the quartz vein in an otherwise statically recrystallized rock. Location is shown in (c). (e) Same as (d) but with crossed polars. amph, amphibole; chl, chlorite; ep, epidote; ser. alb, sericitic albite; qtz, quartz.

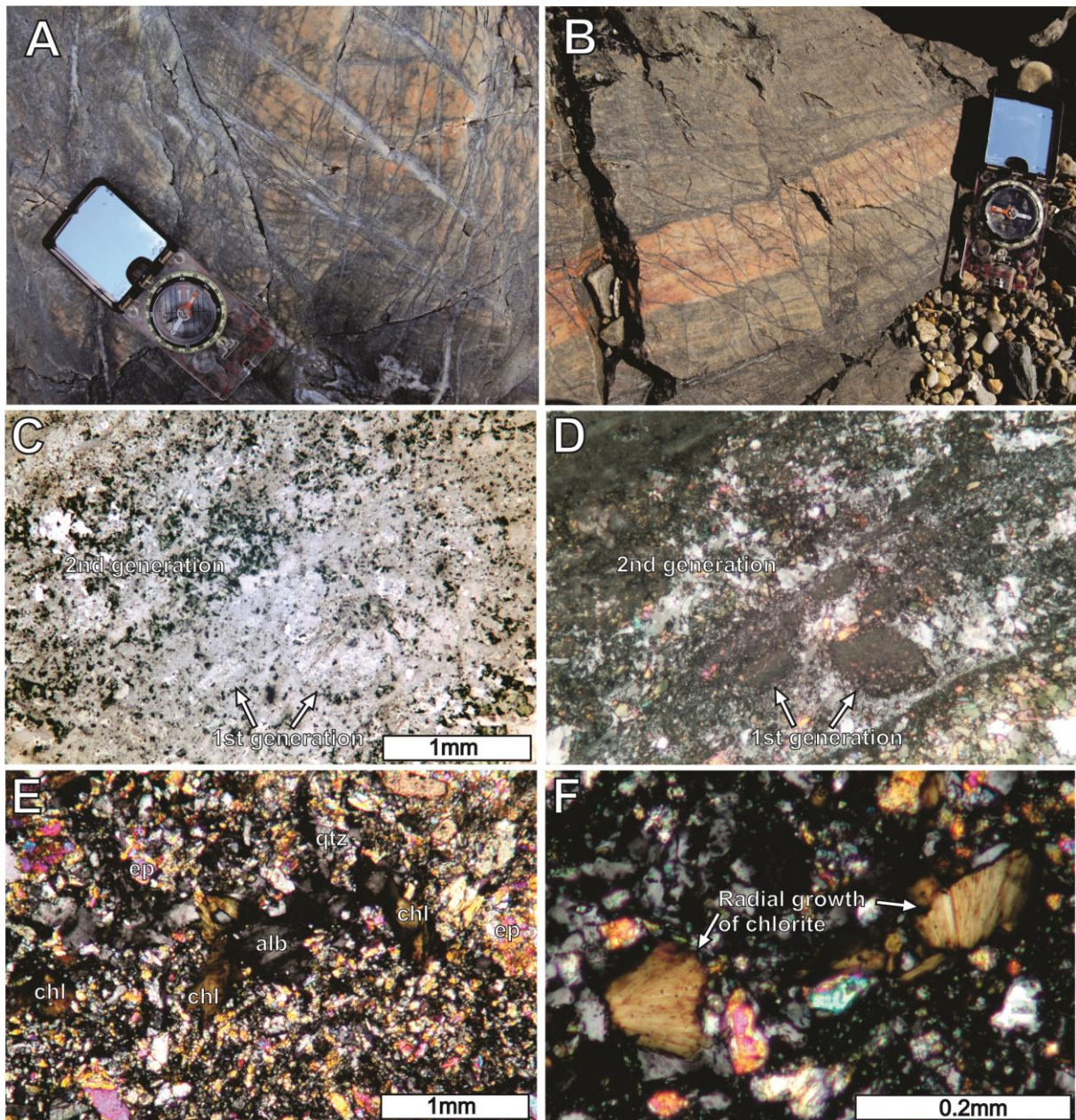


Fig. 8. Outcrop photographs and photomicrographs of cataclastic amphibolitic gneisses from the Kvaløysletta–Straumbukta fault zone at Straumbukta. (a, b) Outcrop photographs of cataclased tonalites from the footwall damage zone of the Kvaløysletta–Straumbukta fault zone. The dark bands of chlorite should be noted. (c) A cataclastic zone showing at least two generations of mafic cataclasite outlined by very fine-grained (<1 μm) epidote, chlorite and quartz aggregates forming the first generation, which appear as clasts within a second generation of cataclasite with similar composition. (d) Same as (c) but with crossed polars. (e) Mafic cataclasite showing greenschist-facies mineral growth. The radial growth of chlorite in the matrix of the cataclasite should be noted. (f) Close-up of chlorite within the cataclasite showing radial growth. Crossed polars. alb, albite; chl, chlorite; ep, epidote; qtz, quartz.

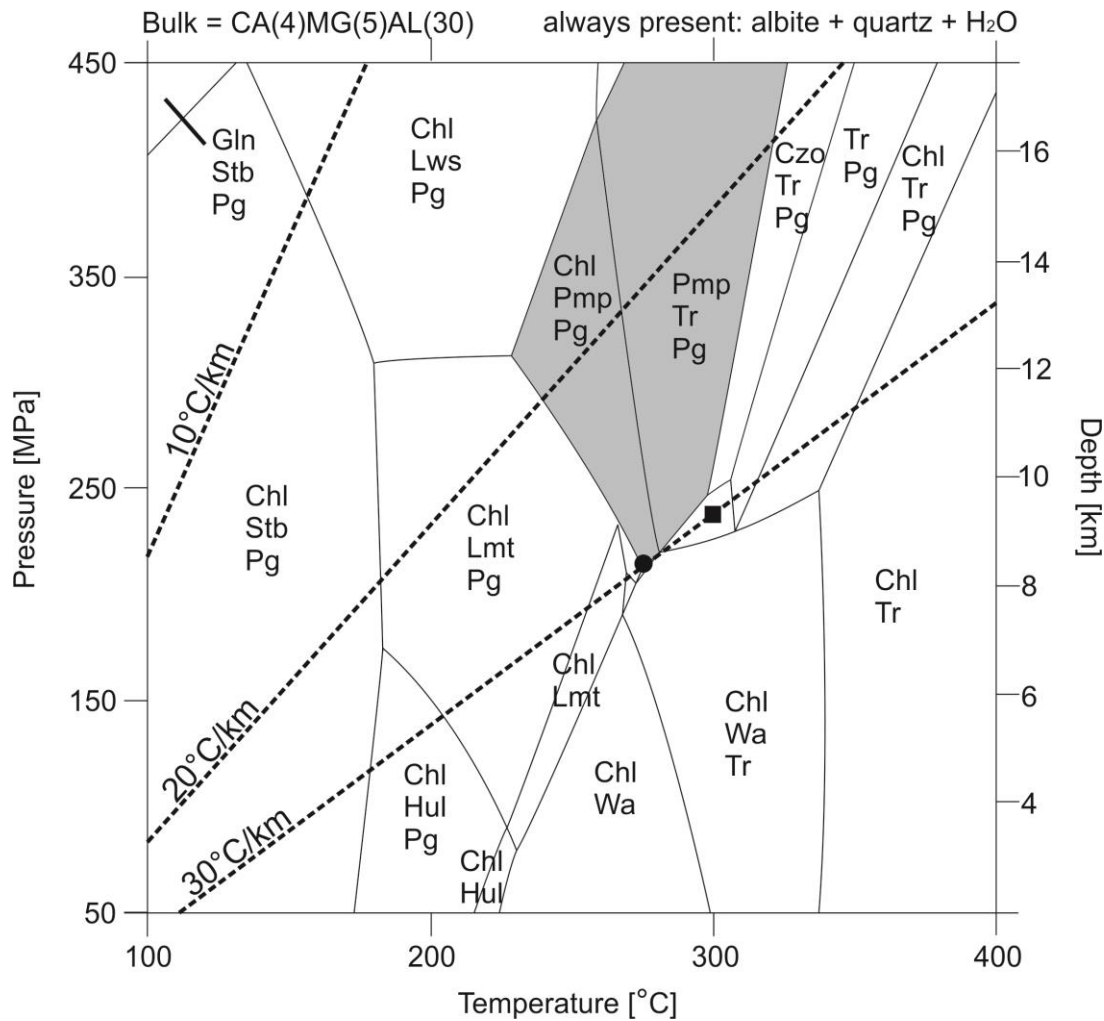


Fig. 9. *P-T* diagram showing mineral assemblages and stability fields of a CMASH system at low-grade metamorphic-facies conditions assuming an average meta-MORB composition. Dashed lines are geothermal gradients. The shaded area marks the stability field of pumpellyite. The black square indicates minimum *P-T* conditions for the early stage faulting; the black circle indicates minimum *P-T* conditions during later-stage faulting. The diagram is modified from Bucher & Grapes (2011). Chl, chlorite; Czo, clinozoisite; Gln, glaucophane; Hul, heulandite; Pg, paragonite; Pmp, pumpellyite; Lmt, laumontite; Lws, lawsonite; Stb, stilbite; Tr, tremolite; Wa, wairakite.

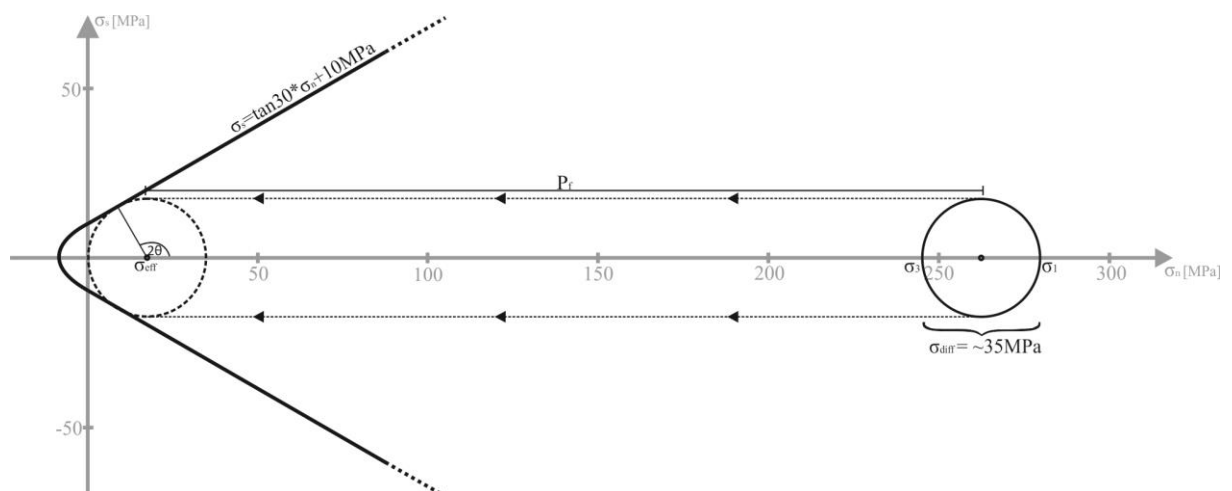


Fig. 10. Mohr diagram showing calculated stress conditions during faulting and a common Mohr–Coloumb failure criterion (see Goodman 1989). The evidence for lithostatic pore pressure suggests that the differential stress did not exceed *c.* 35 MPa.

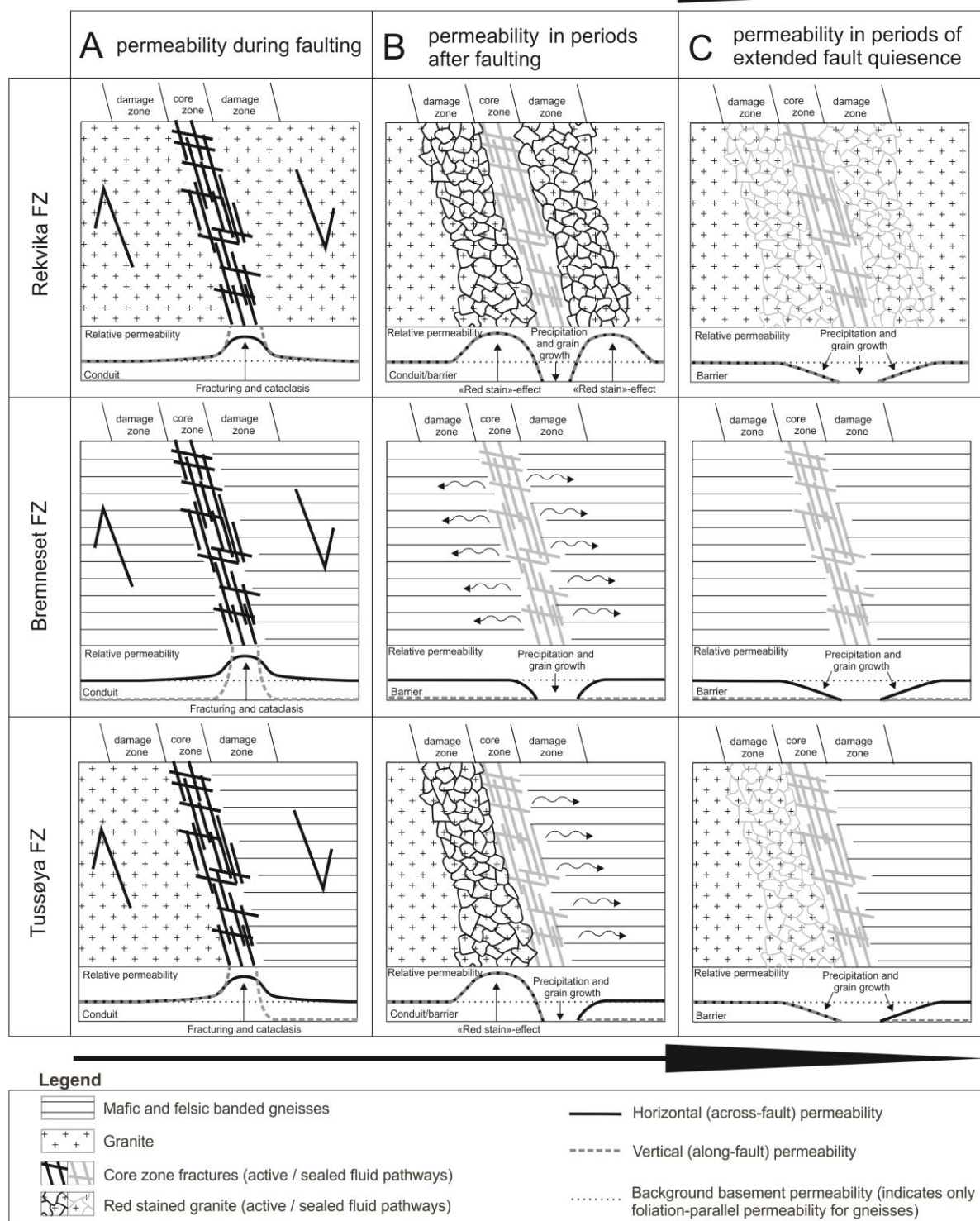


Fig. 11. Schematic illustrations of a model for cyclic changes in permeability contrast through time within fault zones of different host rock lithologies. Relative changes in across-fault and along-fault permeability are illustrated by the curves below each sketch. (a) With faulting, movement along a fault causes fracturing and cataclasis within the core zone and increases permeability. The core zone thereby acts as a fluid conduit. (b) Precipitation of minerals and grain growth within the core zone decreases permeability within the core zone and forces fluid flow into the damage zone. Within feldspar-rich host rocks, permeability increases with time owing to the red staining effect. (c) Grain growth (healing) and precipitation processes through time decrease permeability and with time seal the entire fault zone. Fault reactivation will initiate a new fluid flow cycle.